Combustion and Flame 236 (2022) 111788

Contents lists available at ScienceDirect

Combustion and Flame

journal homepage: www.elsevier.com/locate/combustflame

# Applying heat flux method to laminar burning velocity measurements of $NH_3/CH_4$/air at elevated pressures and kinetic modeling study

Shixing Wang[a,*], Zhihua Wang[b,*], Chenlin Chen[b], Ayman M. Elbaz[a], Zhiwei Sun[c], William L. Roberts[a]

[a] Clean Combustion Research Center, KAUST: King Abdullah University of Science and Technology, Thuwal, Saudi Arabia
[b] State Key Laboratory of Clean Energy Utilization, Zhejiang University, Hangzhou, 310027, China
[c] School of Mechanical Engineering and Centre for Energy Technology (CET), The University of Adelaide, SA 5005, Australia

ARTICLE INFO

*Article history:*
Received 24 April 2021
Revised 25 September 2021
Accepted 25 September 2021
Available online 19 October 2021

*Keywords:*
Ammonia
Methane
High pressure
Laminar burning velocity
Chemical kinetic mechanism

ABSTRACT

Combustion of ammonia ($NH_3$) blended fuels under elevated pressure conditions is critical for adopting this non-carbon fuel in the energy system for decarbonization. In the present work, laminar burning velocities of ammonia/methane($CH_4$)/air mixtures were measured using the heat-flux method at the pressure from 1 to 5 atm with the mixture equivalence ratios ranging from 0.6 to 1.6 and the mole fraction of $NH_3$ ranging from 0 to 1.0. The relatively completed results obtained at elevated pressures were then used for validating and modifying the kinetic mechanisms (CEU-$NH_3$-Mech 1.0) leading to a new version (CEU-$NH_3$-Mech-1.1). Experimental results of $NH_3/H_2$/air in the present work, $NH_3/H_2$/CO/air mixtures measured on the same setup and reported in our previous works were also considered in the development of the kinetic mechanism. It was found that the CEU-$NH_3$−Mech-1.1 can predict well the laminar flame speed, ignition delay time and species concentration in the ammonia oxidation at high temperatures for both $NH_3/CH_4$/air and $NH_3/H_2$/CO/air mixtures in a wide range of equivalence ratios and elevated pressures, including oxygen-enriched combustion conditions. The present experimental results also show that the value of pressure exponent ($\beta$) varies with the mole fraction of ammonia and behaves differently for the mixtures of ammonia blending into $CH_4$ and $H_2$. The kinetic and sensitivity analyses show that the sensitive reactions for $\beta$ are weakly correlated to those for the laminar burning velocity, indicating that $\beta$ can also work as a potential parameter for validating kinetic mechanisms. Ammonia content in the $NH_3/CH_4$/air mixtures determines the pressure exponent variation at over-rich equivalence ratios and reaction pathway variation in the post-flame zone. This work also clarifies the utilization of ammonia containing fuels in rich-lean combustion strategies.



## 1. Introduction

The increasing need to reduce greenhouse gases (GHC) emissions has been accompanied by significant growth in the use of renewable energy sources, *e.g.*, according to the latest International Energy Agency (IEA) report, the share of renewables in global electricity generation jumped to 29% in 2020 [1]. As a carbon-free fuel, ammonia ($NH_3$) has the advantage of lower cost for energy storage and transportation, higher volumetric energy density, easier synthetization from hydrogen, and better commercial viability [2], making it attractive as a potential for future fuel [2,3], *e.g.,* in gas turbines, internal combustion engines and industrial furnaces [4,5] and for power generation. However, the combustion of pure $NH_3$ includes serious challenges related to its low laminar burning velocities [6], long ignition delay times [7], and potential high $NO_x$ emission levels [8,9]. In this sense, it is imperative to develop new combustion technologies to overcome the drawbacks of combustion in this carbon-free fuel, *e.g.,* co-burning with other fuels such as hydrogen and natural gas, and reliable chemical kinetic mechanisms are required for these processes. Ammonia/methane dual fuels have also been successfully applied in two-stage rich-lean combustors to reduce $NO_x$ emissions and increase thermal efficiency [10,11]; they are also promising for utilization in ammonia co-burning.

Laminar burning velocity ($S_L$) is one of the important combustion characteristics for developing and validating chemical kinetic mechanisms and combustion models. Several experimental methods have been developed for $S_L$ measurement, such as an outwardly spherical propagating flame method, a stagnation/counterflow flame method, a heat flux method, an annular stepwise

* Corresponding authors.
*E-mail addresses:* shixing.wang@kaust.edu.sa (S. Wang), wangzh@zju.edu.cn (Z. Wang).

https://doi.org/10.1016/j.combustflame.2021.111788
0010-2180/

diverging tube, an externally heated diverging channel method and a conical flame method [12]. Several results were reported for $NH_3$/air flames [13–16], mostly under atmospheric pressure. The relative scarcity of $S_L$ data, and its dispersion among different measurements, limit the validation of kinetic mechanisms. Blends of ammonia with hydrogen [17–22], methane [22,23] and syngas [24,25] have also been studied under atmospheric and elevated pressures. At the same time, laminar burning velocity data for high $NH_3$ content flames are still rare, particularly under high-pressure conditions. Hayakawa et al. [6] reported $S_L$ data for $NH_3$/air flames up to 5 atm, which showed high buoyancy instabilities; they found that $S_L$ decreased with increasing pressure. Okafor et al. [26] investigated $NH_3/CH_4$/air flames at pressures up to 5 atm and found that the OH radical affected both laminar burning velocity and NO formation. Ichikawa et al. [19] also studied stoichiometric $NH_3/H_2$/air flames up to 5 atm and found that $S_L$ decreased non-linearly with increased ammonia content in the fuel mixture, and that detailed mechanisms–like those of Lindstedt et al. [27], Miller et al. [28] and the GRI-Mech [29]–could not quantitively predict most of the data. Previously reported results of elevated pressures are valuable for developing and validating the chemical kinetic mechanism of ammonia combustion, but some limitations remain. For example, the mole fraction of ammonia was usually kept to low values to stabilize ammonia-blending flames; the equivalence ratio of flames was only slightly varied around the stoichiometric conditions. Therefore, new experimental results for broader combustion conditions at elevated pressures are still required. A recently established high pressure heat flux burner could provide a series of reliable experimental laminar burning velocities for hydrocarbons/syngas/ammonia mixtures etc. [25,30,31], making it worthwhile to advance the high-pressure $S_L$ database of ammonia-blends fuels for kinetic mechanism development.

Except for laminar burning velocity, many other parameters are important for mechanism validation. Xiao et al. [32] investigated ignition delay times (IDT) in ammonia/methane mixtures using a shock tube at five atm; they found that the IDT decreased as pressure and temperature increased, but not sensitive to the change in equivalence ratio with a 10% methane addition—the most effective for decreasing IDT. Oxygen-enriched combustion (OEC) can significantly enhance flame propagation speed and is beneficial in increasing the low reactivity of ammonia; however, the related ammonia oxidation mechanisms have not been fully validated under OEC conditions. Mei et al. [33] measured $S_L$ of the oxygen-enriched $NH_3/O_2/N_2$ flames up to 5 atm using a constant volume chamber. The authors found that oxygen enrichment increased the adiabatic flame temperature and the $S_L$. An ammonia combustion kinetic mechanism, termed CEU-$NH_3$−Mech 1.0 was recently developed and released in [34], which can reasonably predict the combustion of ammonia blending mixture with methane, syngas, methanol and ethanol at atmospheric pressure. Still, its performance for ammonia/methane is not as good as the Konnov mechanism [35]. To explore the interpretation and further validate the CEU-$NH_3$−Mech at elevated pressures, more experimental results of $S_L$ for ammonia/methane mixtures are also needed.

Therefore, the present work aims to apply the heat flux method to measure the laminar burning velocities of $NH_3/CH_4$/air premixed flames with varying the mole fraction of $NH_3$, equivalence ratio and pressure. Second, evaluate the prediction accuracy of various available kinetic mechanisms and further develop the CEU-$NH_3$ mechanism to predict the combustion of $NH_3/CH_4$/air and $NH_3/H_2$/air accurately at elevated pressures. Third, understand the chemical roles of methane and ammonia in the oxidation of their mixture at different pressures by conducting kinetic and sensitivity analysis.

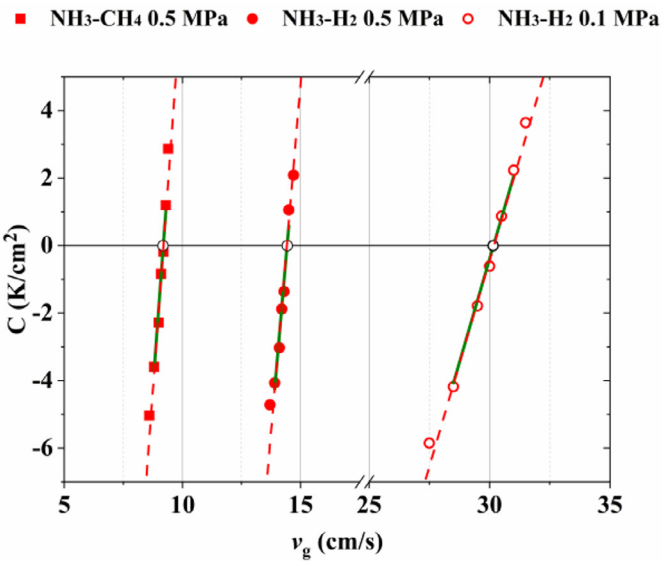


**Fig. 1.** Measured values of $C$ as a function of gas flow rate with a line for $C(v_g) = 0$ to derive the value of for $S_L$ for $NH_3/CH_4$/air and $NH_3/H_2$/air flames with $X_{NH3} = 0.6$ at 1 and 5 atm.

## 2. Experiments

A pressurized chamber, installed with a heat flux burner was used to measure $S_L$ at elevated pressures. Details of the set-up and measurement uncertainties can be found in previous publications [25,30]. Briefly, the chamber has a volume of 35 L, with a maximum sustained pressure of 5 MPa. Pressure in the chamber is controlled by a manually operated valve and an electrical proportional integral derivative (PID) controlled valve, installed in the exhaust gas pipe. A corrosion-resistant mass flow controller (MFC) was used for the $NH_3$ stream. An adiabatic condition was accomplished in the heat flux method because the heat loss from the flame to the burner was compensated by the heat gain from the unburnt mixture with an external circular heater [36]. This method has already been applied separately to the measurement at elevated pressures for hydrocarbons, syngas and ammonia [25,30,31]. The heat flux burner chamber temperature was constant at 298 K, using a thermostatic water bath. A thermostatic oil bath was also used to maintain the burner plate temperature at around 413 K, to stabilize flat flames under elevated pressures. The radial distribution of the temperature over the burner plate can be expressed by Bosschaart and de Goey [37,38]:

$$T_P(r) = T_{center} + C \cdot r^2 \quad (1)$$

where $r$ is the radial distance from the center of the burner plate and $C$ is the parabolic coefficient for a given cold gas velocity of $v_g$. When the gas feeding velocity, $v_g$ was adjusted to maintain constant burner plate temperature (*i.e.*, $T_p(r) = T_{center}$), the adiabatic condition with $C = 0$ and $S_L = v_g$ was achieved [37,38]. Figure 1 illustrates representative results for determining $S_L$ from $C(v_g) = 0$ for $NH_3/CH_4$/air and $NH_3/H_2$/air flames with $X_{NH3} = 0.6$ for 1 and 5 atm. For most flames studied in the present work, at least five points, containing both super-adiabatic and sub-adiabatic conditions were used for the $S_L$ determination by linear interpolation, as shown in Fig. 1. The tilting edge of the ammonia/air flames were alleviated as pressure increased, while flame flicker was aggravated. Both of these two cases were within the intrinsic fluctuations of the temperature measurements by thermocouples.

## 3. Kinetic mechanism and simulations

The first version of CEU-$NH_3$ mechanism, termed CEU-$NH_3$-Mech 1.0 was developed and validated against laminar burning velocity, ignition delay time, and the $NO_x$ emission characteristics in the $NH_3$, $NH_3/CH_4$, $NH_3/H_2$, and $NH_3$/syngas, $NH_3$/methanol and ethanol systems [34]. It adopts $H_2$/CO chemistries from the ELTE-mechanism [39], which was successfully validated under high-pressure syngas $S_L$ conditions. It extracted the C1-C4 species from the San Diego mechanism [40] and updated the C/N interaction reactions from the Konnov mechanism [35]; it was also tuned for methanol/ethanol oxidation.

Based on the sensitivity and reaction pathway analyses, the three reactions below were updated to predict better flame speed and $NO_x$ formation during ammonia/methane co-oxidation. The first reaction is $NH_2 + O = H + HNO$ with adopting the rate constants of Inomata and Washida [41], which were also used in the Konnov mechanism [35]. Shrestha et al. [42] observed that $NH_3/H_2$ flame speed was highly sensitive to this reaction with increasing $H_2$ in the blend. Our sensitivity analyses also showed that this reaction played a key role in changing the flame speed of ammonia/methane blends with medium ammonia content. This reaction is also important in predicting high temperature NO formation, as pointed out by Glarborg et al. [43]. The other two reaction are branching reactions, *i.e.*, that $NH + NO = N_2O + H$ and $NH + NO = N_2 + OH$ with adopting the rate constants and branching ratio of Baulch et al. [44] to improve $N_2O$ prediction performance. These rate coefficients agree well the theoretical and experimental work (within the uncertainty), as suggested by Glarborg et al. [43].

Other detailed mechanisms were also used for the $NH_3/CH_4$/air premixed flames, including the GRI-Mech 3.0 [29], mechanisms developed individually by Okafor et al. [23], San Diego [45], Mendiara and Glarborg [46], Glarborg et al. [43] and Capriolo et al. [35]. Two more recently established mechanisms were also used here. The one developed by Shrestha et al. [42] which compiled kinetic model for predicting the oxidation of ammonia oxygen-enriched combustion and ammonia-hydrogen blends. Arunthanayothin et al. [47] developed ammonia/methane co-oxidation mechanisms that were based on the ammonia oxidation mechanism of CRECK [48], and combined with C0-C3 mechanisms. This mechanism was validated against the low temperature (below 1200 K) jet-stirred reactor (JSR) data and high temperature flow reactor data. In the following sections, these kinetic mechanisms mentioned above are termed *GRI-Mech 3.0, Okafor-Mech, UCSD-Mech, Mendiara-Mech, Glarborg-Mech, Konnov-Mech, Shrestha-Mech* and *CRECK-Mech*.

$S_L$ predictions, and species concentrations were conducted using the PREMIX module of the CHEMKIN 2019 [49]. The simulated flue gas emissions were conducted with the burner stabilized flame (BSF) module and plug flow reactor (PFR). Ignition delay time was simulated in a closed homogenous reactor, while the ignition delay times were derived from criteria in the literature with corresponding experiments. For $S_L$ simulation, an adaptive regridding method, with convergence conditions of GRAD and CURV values setting at 0.02 (ensuring at least 500 grid points), was used for both flame speed calculation and emissions simulation. Thermal diffusion (the Soret effect) and mixture-averaged transport formulation were included in the computations.

The following contents of the paper is structured as below: in the Section 4, we test the different mechanisms against the present flame speed data at different mole fractions (Section 4.1), different equivalence ratios (4.2) and different pressures (4.3), specially, we introduced the pressure exponent, $\beta$, to validate different mechanisms' accuracy and analyzed the pressure dependence of different fuel mixture types; The CEU-$NH_3$-Mech 1.1 is validated in a wider range of literature data in Section 4.4; Section 4.5 is the sensitivity and kinetic analyses followed by the Section 4.6 over-rich behavior of $NH_3/CH_4$/air flames.

## 4. Results and discussion

### 4.1. Effect of ammonia mole fraction on laminar burning velocity

Figure 2 shows the laminar burning velocities of stoichiometric $NH_3/CH_4$/air flames as a function of $X_{NH3}$ measured at the different pressures of 1, 3 and 5 atm. The figure also presents other experimental data available in literature and the results predicted by the eight ammonia oxidation mechanisms (mentioned above), as well as the CEU-$NH_3$-Mech 1.1. The data revealed that the measured $S_L$ for the $NH_3/CH_4$/air flames decreased almost linearly as $X_{NH3}$ increased. The eight kinetic mechanisms predicted the experimental data for the $NH_3/CH_4$/air flames well, especially for those with low and high $NH_3$ content, except Glarborg-Mech. It was found that at one atm, the Okafor-Mech, UCSD-Mech and CEU-$NH_3$-Mech 1.1 performed better than the other mechanisms. While at elevated pressures of three and five atm, the Okafor-Mech and UCSD-Mech underpredicted the flame speed near the side of neat methane, for which the CRECK-Mech, Konnov-Mech and CEU-$NH_3$-Mech 1.1 mechanisms showed better agreement with our present experimental data. Near the side of neat ammonia, Okafor-Mech and Konnov-Mech overpredicted the flame speed of high ammonia-content mixtures, while the UCSD-Mech, CRECK-Mech and CEU-$NH_3$-Mech 1.1 mechanisms displayed better agreement with the experimental results. It was noted that these three mechanisms UCSD-Mech, CRECK-Mech and CEU-$NH_3$-Mech 1.1 under-predicted the pure ammonia flame speed of the present work, but due to the higher experimental uncertainty in the $S_L$ measurement for pure ammonia, the data reported by Hayakawa et al. [6] offered acceptable agreement with these three mechanisms. The CEU-$NH_3$-Mech 1.1 predicted better at medium ammonia content than the CRECK-Mech and better than the other mechanisms.

The previous study has shown that the performance of mechanisms predicting ammonia/methane and ammonia/hydrogen may differ substantially because $NH_3/H_2$/air flames have higher diffusivity and reactivity than $NH_3/CH_4$/air flames. It is helpful to validate mechanisms by targeting ammonia/methane and ammonia/hydrogen together under elevated pressures, which has been rarely reported. Therefore, ammonia/hydrogen data are also included in Fig. 3 (a–c) to assure that the mechanisms which performed well on ammonia/methane can also work for ammonia/hydrogen. Measurements have not conducted for $NH_3/H_2$/air flames with $X_{NH3} \leq 0.4$ due to the limitations of the heat flux method and the cellular flame instability effects. The heat flux method has an upper measuring limit of 60–80 cm/s due to the burner plate's small scale curvature and inhomogeneous transport effects [50]. Thus, it is unsuitable for high-hydrogen-content mixtures.

However, flames with high hydrogen content mixtures at elevated pressures are assumed to have thermal-diffusive instability (Lewis number less than one) and hydrodynamic instability (*i.e.*, density jumps across the flame front due to thermal expansion), thinner flame thickness aggravates this effect. Thus, the laminar flame speed of hydrogen-air flames at very high pressures is rarely reported, while hydrogen flames diluted with helium occur more often. Figure 3 (a–c) shows that the measured $S_L$ values (in log scale) for the $NH_3/H_2$/air flames features an exponential decrease, with $X_{NH3}$ at both 1, 3 and 5 atm. $H_2$-air flame speed data are also provided first to validate the mechanism's accuracy with neat hydrogen at elevated pressures. Almost all the present mechanisms predicted the hydrogen flame speed well, except Glarborg-Mech. Although the eight kinetic mechanisms predicted

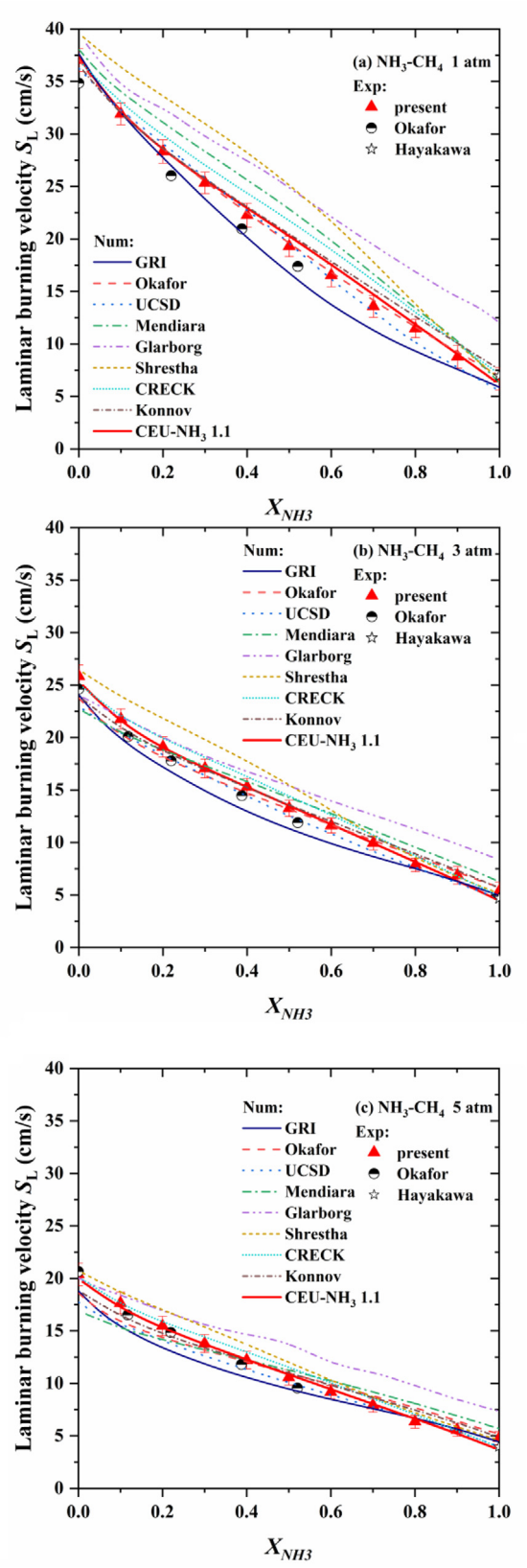


**Fig. 2.** Measured and predicted laminar burning velocities of stoichiometric $NH_3/CH_4$/air flames as a function of $X_{NH3}$ at one, three and five atm and 298 K. Data in the literature from Okafor et al. [26] and Hayakawa et al. [6].

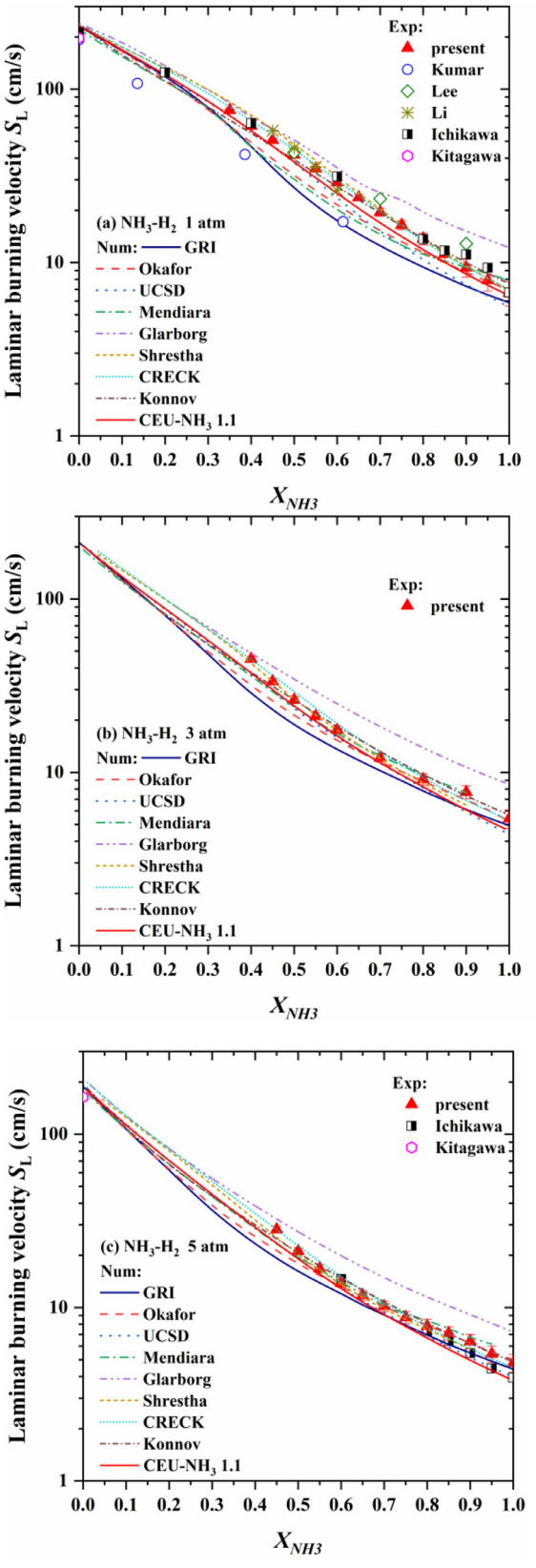


**Fig. 3.** Measured and predicted laminar burning velocities of stoichiometric $NH_3/H_2$/air flames as a function of $X_{NH3}$ at one, three and five atm and 298 K. Data in the literature from Ichikawa et al. [19], Kumar and Meyer [17], Lee et al. [20], Li et al. [18] and Kitagawa et al. [53].

well against experimental data for the $NH_3/CH_4$/air flames relatively well–especially for those with low and high $NH_3$ content–some discrepancies were observed for medium fuel blend ratios in both $NH_3/CH_4$/air and $NH_3/H_2$/air flames, and predictions varied widely among the different mechanisms, especially for $NH_3/H_2$/air flames. It was found that the Okafor and the GRI-Mech 3.0 performed well with the $NH_3/CH_4$/air flames, but they underpredicted the values of $S_L$ in $NH_3/H_2$/air flames. This is because the Okafor-Mech initially adopted the $H_2$/CO sub-mechanism from the GRI-Mech 3.0, which has shown not an accurate prediction of $H_2$/CO mixtures for flame speed under high pressures up to 20 bar [51,52]. The CEU-$NH_3$-Mech 1.1 adopted updated $H_2$/CO chemistry and the same hydrocarbon chemistry as UCSD-Mech and different ammonia chemistry. Still, they both perform better than GRI-Mech and predict similar flame speeds for $NH_3/H_2$/air shown in Fig. 3, which implies the overall prediction accuracy for stoichiometric cases lies more on hydrocarbon chemistry than on ammonia chemistry.

Although the CRECK-Mech gave better agreement with experimental results of $NH_3/H_2$/air conditions at elevated pressures, it overpredicted the atmospheric $NH_3/H_2$/air, and all $NH_3/CH_4$/air flame speeds. It was found that the Konnov-Mech and CEU-$NH_3$-Mech 1.1 offered better predictions for the flame speed of $NH_3/H_2$/air at medium-ammonia content, where the UCSD-Mech slightly underpredicted the results. Thus, the modification of hydrogen and ammonia chemistries in CEU-$NH_3$-Mech 1.1 resulted in improved $S_L$ prediction in comparison with the original UCSD-Mech at elevated pressures.

### 4.2. Effect of equivalence ratio on laminar burning velocities

Figure 4 (a–c) shows the measured and predicted laminar burning velocities of $NH_3/CH_4$/air as a function of equivalence ratio $\phi$ for different $X_{NH3}$ at 1, 3 and 5 atm. Figure 4(d) shows the previous $NH_3$/syngas/air flames data with molar fraction of $NH_3$: $H_2$: CO = 0.6: 0.2: 0.2. The predictions based on the modified CEU-$NH_3$-Mech 1.1 and the original version are presented and compared to validate the mechanism's accuracy for both $NH_3/CH_4$ and $NH_3$/syngas at elevated pressures. It was found that adding $CH_4$ greatly enhanced the fuel mixture flame speed under lean and stoichiometric conditions, while measured and simulated laminar burning velocities agree well for different ammonia content under rich conditions. The CEU-$NH_3$-Mech 1.1 and Konnov-Mech presented a better agreement for stoichiometric flame speed predictions at elevated pressures. Previous work showed that the Konnov-Mech gave better predictions than CEU-$NH_3$-Mech 1.1 for $NH_3/CH_4$/air flames in a wide range of equivalence ratios under atmospheric pressures. It can be seen in Fig. 4(a–c) that the modified CEU-$NH_3$-Mech 1.1 predicted flame speed better than the previous version with various ammonia content from $X_{NH3}$ = 0.2 to 0.6–especially under atmospheric pressure–and the difference between these two mechanisms decreased with increasing pressure, due to the decrease in the overall magnitude of $S_L$. The modified mechanism also responded better at rich equivalence ratios than the Konnov-Mech.

In Fig. 4(d), it was found that both the two CEU-$NH_3$ mechanisms better predicted the $S_L$ of the $NH_3/CH_4$/air flames than those of the $NH_3$/syngas/air flames, for all the pressure and equivalence ratios studied. Both of the two CEU-$NH_3$ mechanisms underpredicted the laminar burning velocity of the $NH_3$/syngas/air at lean and stoichiometric sides, while the Konnov overpredicted the results at the rich side. Back to the $NH_3/CH_4$/air mixtures, it was observed that the over prediction of $S_L$ for rich mixtures is aggravated with the increase of $X_{NH3}$ or the pressure. Considering the fully validated hydrocarbon chemistry will not induce such large discrepancies in flame speed prediction at rich equivalence ratios, and this discrepancy only happens at high ammonia contents; This note, together with previous work [25] and the current sensitivity analysis in Section 4.5, showed that the $NH_2$ related chain-propagating reactions $NH_2$+O/H/OH→HNO/NH and recombination reactions $NH_2$+NH→$N_2H_i$ become more critical as $X_{NH3}$ increases or $\phi$ increases. The rate constants of these reactions play the dominant role in affecting the prediction accuracy of flame speed of ammonia/hydrocarbon mixtures.

Thus, the modified CEU-$NH_3$-Mech 1.1 improved prediction accuracy–especially at the rich side–at elevated pressure by adjusting the ammonia chemistry. This also means that discrepancies between measurements and predictions were controlled by the hydrocarbon and hydrogen chemistries in flames with low ammonia content, and dominated by ammonia chemistry in flames with high ammonia content. Overall, the present CEU-$NH_3$-Mech 1.1 displayed a noticeable improvement in laminar flame speed predictions of $NH_3/CH_4$/air and $NH_3$/syngas/air at elevated pressures.

### 4.3. Pressure power exponent analysis

Figure 5 shows the measured and predicted laminar burning velocity $S_L$ of stoichiometric $NH_3/CH_4$/air as a function of pressure for different $X_{NH3}$. $S_L$ values of all fuel mixtures decreased gradually as the pressure increased; the decrease of the values of $S_L$ of $CH_4$/air were more obvious than those of $NH_3$/air flames. The present mechanism predicted the values of $S_L$ more accurately than the original CEU-$NH_3$-Mech 1.0, especially at high ammonia content. As the pressure increased, discrepancies among the different mechanisms were reduced for $NH_3/CH_4$/air flames. Furthermore, as the ammonia content in the fuel mixture increased, discrepancies among the different mechanisms also increased and were maximized at medium ammonia content, $X_{NH3}$ = 0.4∼0.6. The Konnov-Mech predicted better with high-methane-content mixtures and the CEU-$NH_3$-Mech 1.1 predicted better with high-ammonia-content mixtures, especially at elevated pressures. For medium-ammonia-content mixtures, the modified CEU-$NH_3$-Mech 1.1 and the Konnov-Mech predicted similarly, so the interaction between ammonia chemistry and hydrocarbon chemistry was accurately described at elevated pressures.

The exponents $\beta$ are defined in equation $S_L/S_{L0} = (P/P_0)^{\beta}$, where $P_0$ and $S_{L0}$ represent the initial pressure and $S_L$ at one atm. The pressure power exponent $\beta$ was related to the overall reaction order $n$ in $S_{L0} \propto P^{\frac{n}{2}-1}\exp(-\frac{E_a}{2R_0T_{ad}})$ through $\beta$ = n/2–1. Therefore, the pressure effect on the chain mechanism could be identified and quantified through $\beta$. For a given flame condition, the decrease in the laminar burning velocity with pressure as indicated by the current data or from the literature are highlighting the importance of the pressure sensitive chain mechanisms in the process of the flame propagation. For example, the chain branching reaction, H + $O_2$ = OH + O, is a two-body reaction with high sensitivity to temperature, while the three body-body reaction H + $O_2$ + M = $HO_2$ + M showed less sensitivity to temperature but a high sensitivity to pressure (inhibiting reaction). Increasing the pressure enhanced the three-body reaction relative to the two-body branching reaction; thus, a retarding impact is imposed on the overall reaction. It is worth noting that, considering the increased mixture density with pressure the decrease in the laminar burning velocity with pressure is not due to the chain-termination reactions but also the high density with pressure has a critical rule. Given that the overall reaction order $n$ should approach close to 2 as pressure decreases due to the dominant effect of the two-body reactions compared to the three-body termination reactions. However, as the pressure increases, due to the existence of three-body termination reactions, $n$ should be smaller than 2. This is because while the order of the termination reaction can be 3, its effect on

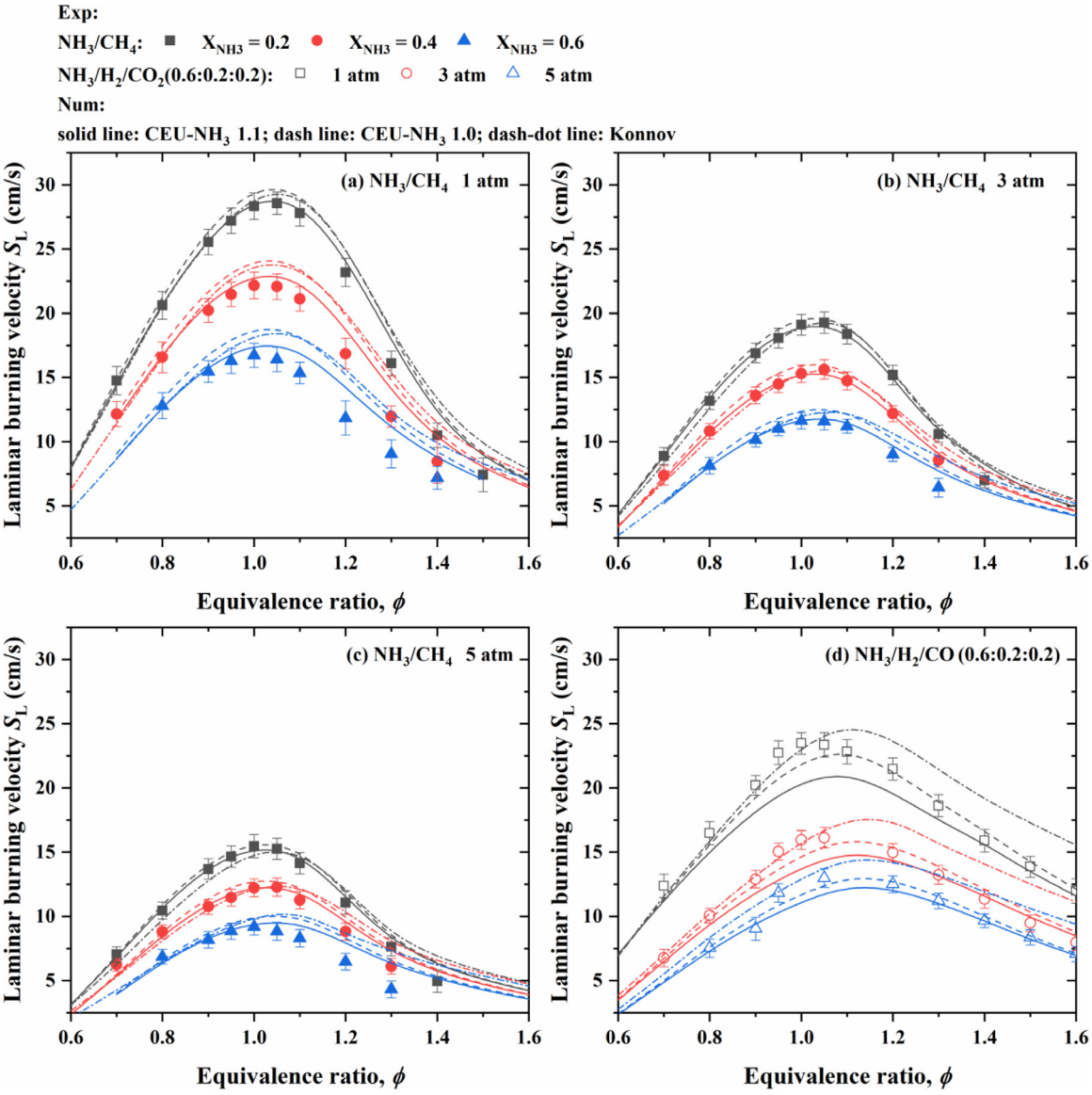


**Fig. 4.** Measured and predicted laminar burning velocities of (a)(b)(c) $NH_3/CH_4$/air as a function of $\phi$ for different $X_{NH3}$ at one, three and five atm and 298 K, and (d) $NH_3$/syngas/air flames [25].

the overall reaction order is negative, and thus $\beta$ is less than zero (as will be shown in Figs. 6, 7). The detailed uncertainties calculation for flame speed measurements at different pressures are expanded in our previous work [25]. The uncertainty of the pressure exponents is also shown in the figure as the error bar. Briefly, the $\beta$ was calculated as the slope of the linear regression of $\ln(S_{Li}/S_{L0})$ versus $\ln(P_i/P_0)$ [12] based on the least squares method, and thus $\beta$ is a function of individual burning velocities at each pressure, $S_L^{P_i}$, and $\beta = f(S_L^{P_1}, S_L^{P_2}, \ldots, S_L^{P_n})$. According to this expression of $\beta$ and the obtained uncertainty in flame speed, $\Delta S_L^{P_i}$, the uncertainty of $\beta$ was calculated following the error propagation formula:

$$\Delta\beta = \frac{\left(\sum_i \left[\left(ln\frac{P_i}{P_0} - \overline{ln\frac{P_i}{P_0}}\right)\cdot\frac{\Delta S_L^{P_i}}{S_L^{P_i}}\right]^2\right)^{0.5}}{\sum_i ln^2\frac{P_i}{P_0} - n\cdot\left(\overline{ln\frac{P_i}{P_0}}\right)^2} \quad (2)$$

where $P_0$ is the initial pressure one atm, and $P_i$ is the $i^{th}$ pressure value used to derive $\beta$ over total pressures and flame speeds. Figure 6 illustrates variation of the pressure power exponent, $\beta$, of stoichiometric mixtures for $NH_3/CH_4$/air mixture (Fig. 6a) and for $NH_3/H_2$/air mixtures (Fig. 6b) with $X_{NH3}$. It can be seen that $\beta$ first decreased and then increased as $X_{NH3}$ increased for $NH_3/H_2$/air while it varies very slightly before $X_{NH3} = 0.5$ for $NH_3/CH_4$/air. It was also found that the present values of $\beta$ agreed well with those from Okafor et al. [26] for $NH_3/CH_4$/air flames, but large discrepancies were observed against the data of Ichikawa et al. [19] for $NH_3/H_2$/air flames. Figure 6 also includes $\beta$ values, calculated using different kinetic mechanisms. It was noted that the value of $\beta$ for pure ammonia was located between those for pure hydrogen and pure methane. The non-linear relationship of $\beta$ with $X_{NH3}$ was also confirmed numerically, and the minimum pressure exponents occurred at conditions with medium ammonia content for $NH_3/H_2$/air; meaning that the flame speed here was more sensitive to pressure change than in low and high ammonia content. For $NH_3/CH_4$/air, both the current and previous CEU-$NH_3$-Mech gave the most accurate predictions with the experimental results for low ammonia content conditions with $X_{NH3} \leq 0.5$; the other mechanisms all underpredicted the pressure exponents near the methane side. However, uncertainty in $\beta$ grew in $X_{NH3} \geq 0.5$

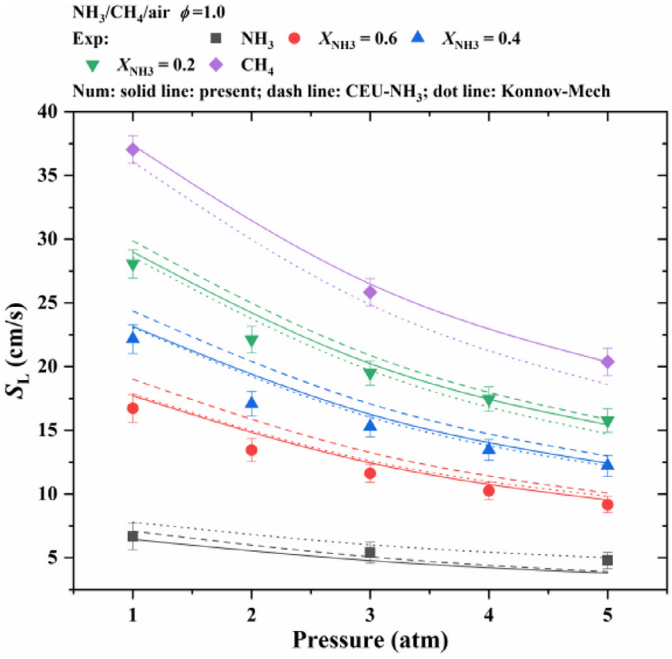


**Fig. 5.** Measured and predicted laminar burning velocities of stoichiometric $NH_3/CH_4$/air flames as a function of pressure for different $X_{NH3}$.

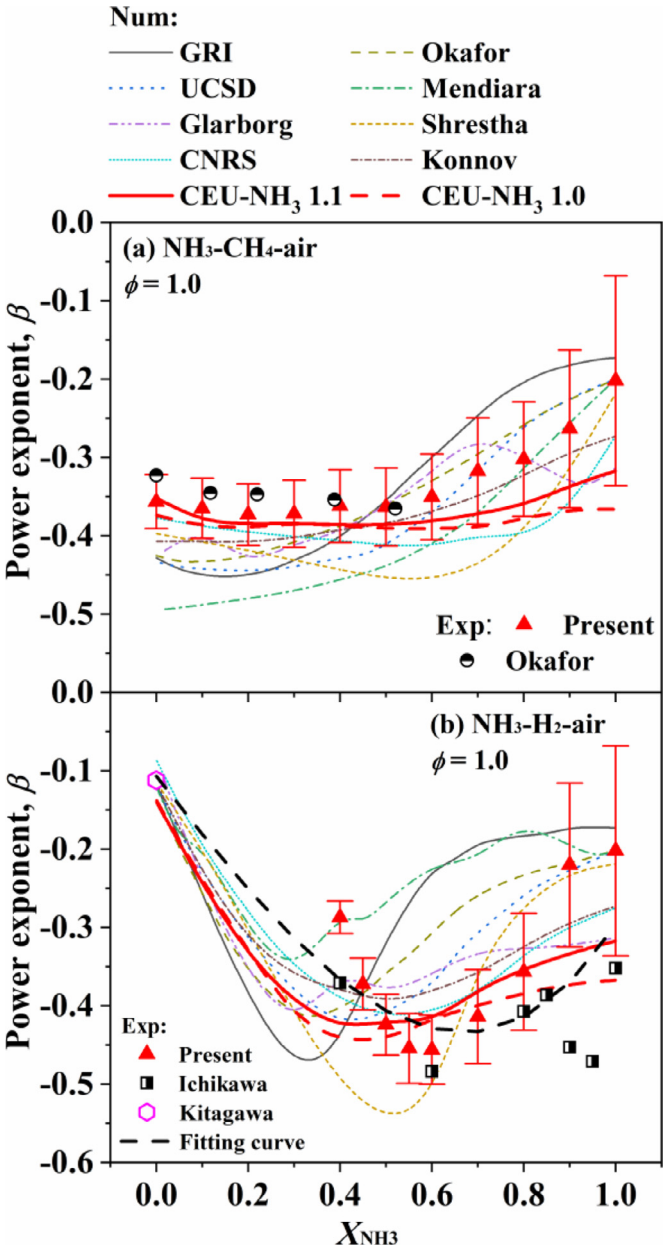


**Fig. 6.** Pressure power exponent of stoichiometric (a) $NH_3/CH_4$/air and (b) $NH_3/H_2$/air flames as a function of $X_{NH3}$. Literature data from Okafor et al. [26], Ichikawa et al. [19] and Kitagawa et al.[53].

conditions as $X_{NH3}$ increased, due to the increasing measurement uncertainty of $S_L$. The CEU-$NH_3$-Mech 1.0 slightly underpredicted the pressure exponents, but the modified CEU-$NH_3$-Mech 1.1 improved the prediction capacity to within the error bar range. For $NH_3/H_2$/air flames, most of the mechanisms failed to capture the minimum $\beta$, but the Konnov, CRECK, and even the Shrestha mechanisms described better the $\beta$ variation for the conditions of $X_{NH3} \geq 0.5$. Although the variation trend of experimental $\beta$ values behave largely different from the simulated results in the range of $X_{NH3} = 0.4$–$0.6$, the fitting curve of experimental results of present work and data from Ichikawa et al. [19] and Kitagawa et al. [53] in Fig. 6(b) agreed well with the numerical results. However, there were still some under-prediction of the pressure dependence of $S_L$ at $X_{NH3} \leq 0.5$ and over-prediction at $X_{NH3} \geq 0.5$, which needs further improvement. The current CEU-$NH_3$-Mech 1.1 shows the most reliable predictions for both $S_L$ and $\beta$. Most of the mechanisms have the biggest prediction divergence for $S_L$ and $\beta$ at $X_{NH3} = 0.2$–$0.6$ for $NH_3/H_2$/air and $X_{NH3} = 0.6$–$1.0$ for $NH_3/CH_4$/air as shown in Figs. 2, 3 and 7 because the net ammonia mass burning rate, $f_{NH3}$ gets maximum at this range ($f_{NH3} \propto S_L \cdot X_{NH3}$). At the same time, the experimental uncertainty is not changed too much over all $X_{NH3}$ and thus this range is beneficial for the mechanism validation and improvement.

Figure 7 presents experimental and numerical pressure exponents of $NH_3/CH_4$/air with different $X_{NH3}$ content as a function of the equivalence ratio; the previous $NH_3$/syngas/air ($NH_3/H_2/CO$=60/20/20) data is also included for comparison. It was found that both the CEU-$NH_3$-Mech 1.0 and 1.1, as well as the Konnov-Mech predicted the values of the pressure exponents well at wide range of equivalence ratios; all their predictions were within the experimental uncertainty. Among these, the present mechanism displayed the most satisfactory prediction accuracy, especially at lean and stoichiometric sides. It can be seen in Fig. 7(a) that $\beta$ had a maximum around $\phi = 1.0$, both experimentally and numerically, which means that improved reactivity with increasing pressure was less significant for slightly rich mixtures than for stoichiometric, or very rich mixtures. The non-monotonic behavior of pressure exponents $\beta$ of hydrocarbon fuels has been explained in previous work [30,54]. However, it can be seen in Fig. 7(a) (b), that when $X_{NH3}$ increased, non-monotonic behavior ceased, which means that at rich equivalence ratios ammonia chemistry changed the pressure dependence of $S_L$ of $NH_3/CH_4$ mixtures. This can be explained by the role of $CH_3$ recombination reactions, which were more retardant than $NH_2$ in the rich flames (discussed in detail in Section 4.5: Sensitivity and kinetic analysis). With the same ammonia content, and because of their similar flame temperature, the value of the pressure exponents of $NH_3/CH_4$ and $NH_3/H_2/CO$ were similar over the wide range of equivalence ratios, and their divergence began at rich conditions. All three mechanisms gave similar prediction results within the experimental uncertainty range; of these, the present mechanism was most accurate, especially at stoichiometric and rich conditions.

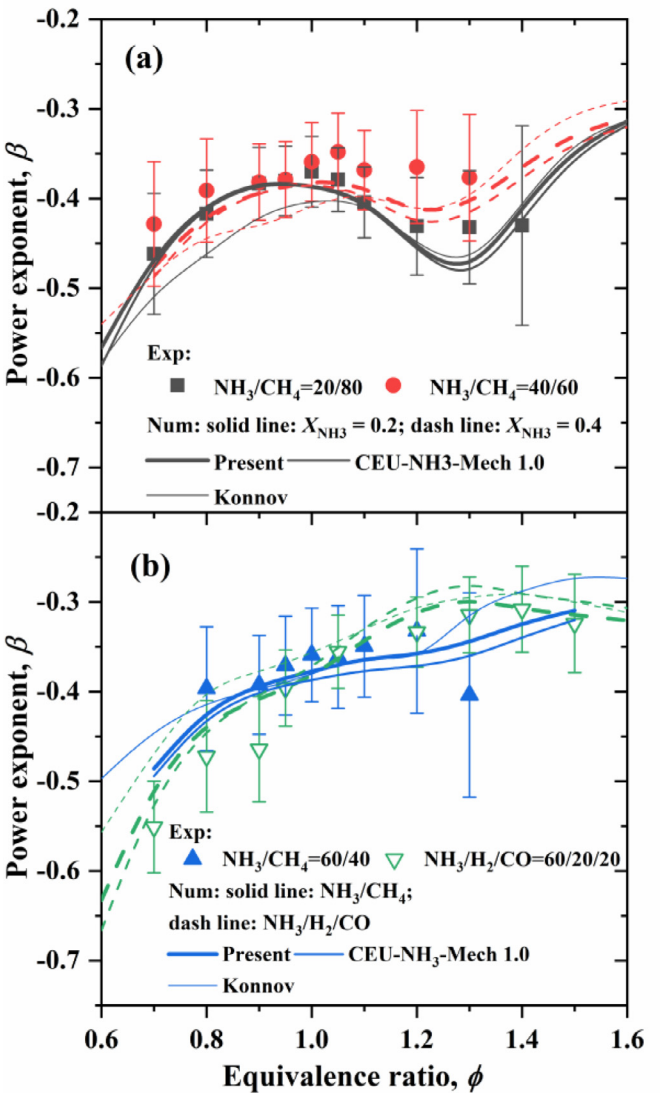


**Fig. 7.** Pressure power exponent of $NH_3/CH_4$/air and $NH_3$/syngas/air flames as a function of $\phi$. Data from Wang et al. [25].

### 4.4. Validating the CEU-$NH_3$ 1.1 mechanism

The present model was not thoroughly validated against ammonia-oxidation measurements under elevated pressures. To demonstrate that the modified model predicted validation experiments from previous work, its performance against the flame speed of oxygen-enriched combustion, OEC, of ammonia, reported in the literature, is presented here. Oxygen-enrichment can significantly accelerate flame propagation in ammonia/air mixtures and reduce buoyancy flame instability in low reactivity fuels [33]. This makes it useful for practical ammonia combustion, and kinetic model validation at elevated pressures; this can help in closing the gap caused by uncertainties in ammonia chemistry. Figure 8(a) and (b) shows that the Shrestha-Mech and CEU-$NH_3$-Mech 1.0 always predicted rich flame speeds better, while over-predicting lean and stoichiometric conditions. After modification, the CEU-$NH_3$-Mech 1.1 agreed with the Konnov-Mech and CRECK-Mech, and agreed better with the experiments in the literature at lean and stoichiometric conditions. The maximum difference between the various mechanisms at $\phi = 1.0$ could reach ten cm/s, indicating the high uncertainty of ammonia chemistry. Regarding OEC conditions at elevated pressures (Fig. 8(c)), it was discovered that the Shrestha and Konnov mechanisms now overpredicted all the flame speeds, as reported in the literature. The previous CEU-$NH_3$-Mech 1.0 predicted well at five atm, but overpredicted at one atm; the present model significantly improved the prediction accuracy at one atm, losing little in the five atm predictions. The CRECK-Mech presented better predictions for both conditions.

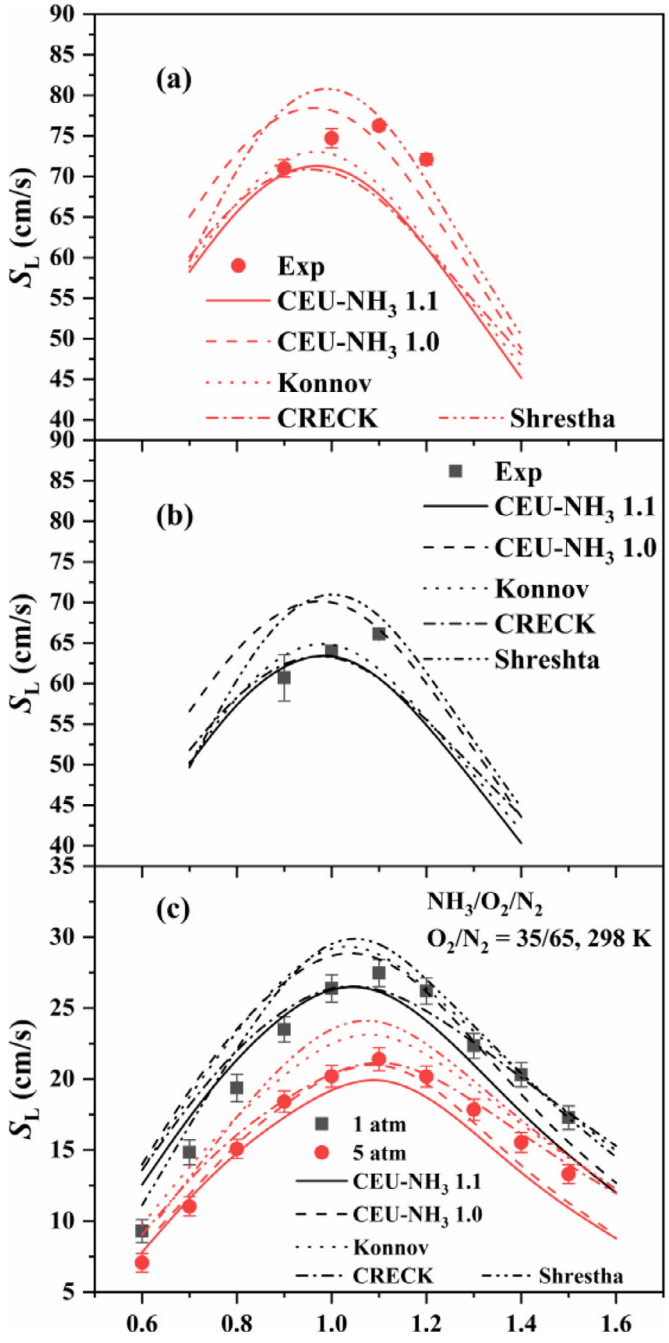


**Fig. 8.** Data from the literature re laminar burning velocity of $NH_3/O_2$/He at one atm and 373 K (a) $X_{O2} = 0.3$, (b) $X_{O2} = 0.27$ (Shrestha et al. [42]); (c) $NH_3/O_2/N_2$ at one and five atm with $X_{O2} = 0.35$ (Mei et al. [33]).

Figure 9 shows the validation of the ignition delay time data of $NH_3/O_2$/Ar and bio-syngas/$NH_3$ at high pressures, reported in the literature, against the four recent mechanisms. Results showed that the present CEU-$NH_3$−Mech 1.1 reproduced

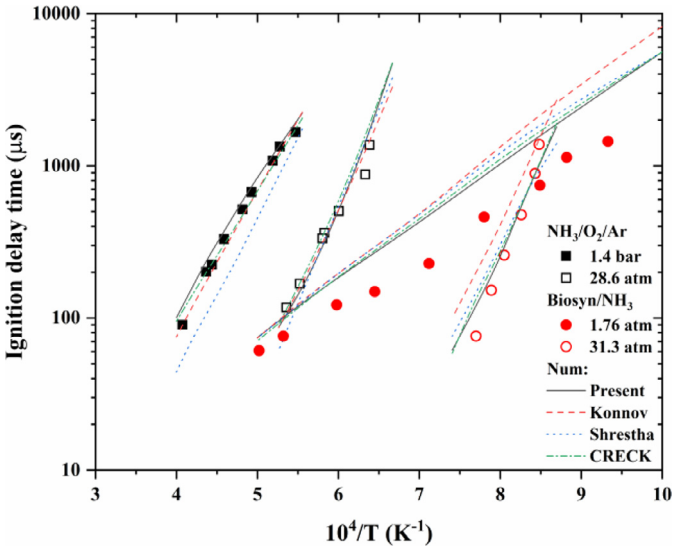


**Fig. 9.** Data from the literature re ignition delay time of $NH_3/O_2/Ar$ flames (0.01143 $NH_3$/0.00857 $O_2$/0.98 Ar) at around 1.4 atm and 28.6 atm [55]; ignition delay times of bio-syngas (molar composition: 0.02%$NH_3$, 0.089%$CH_4$, 0.297%$H_2$, 0.297%CO, 0.21% $H_2O$, 0.157%$CO_2$, 0.95%$O_2$, 97.98%Ar) in a shock tube at 1.76 and 31.3 atm [56].

ignition delay time data well at both normal and high pressures, except that all mechanisms over-predicted the bio-syngas data at 1.76 atm. The Shrestha-Mech slightly underpredicted the atmospheric data of $NH_3/O_2/Ar$, while the Konnov-Mech over-predicted the bio-syngas/$NH_3$ data at low temperatures, from 1000 to 1400 K. Previous studies [34] found that the dominating reactions for ammonia ignition differed from the flame speed; the $H_2NO$ and $NO_2$ chemistries were important at low and intermediate temperatures and the C/N interaction reactions ($CH_4+NH_2=CH_3+NH_3$ and $H_2NO+CH_3=CH_3O+NH_2$), which were almost negligible in terms of affecting the laminar flame speed calculations.

Figure 10(a) shows the emission prediction capacity of the modified and other mechanisms against the experimental data from the literature [57] for $NH_3$/NO/Ar oxidation in a burner stabilized. The Shrestha-Mech gave the most accurate prediction of NO consumption and $N_2$ formation, and of $N_2O$ concentration at the tail of the reaction zone. The CEU-$NH_3$-Mech 1.1, and the CRECK-Mech and Konnov-Mech, predicted the increasing trend of $N_2O$ well, but only the CEU-$NH_3$-Mech 1.1 gave a close prediction of the decreasing trend of $N_2O$ in comparison with the experimental data; some divergence remained, however, which may require further development of the CEU-$NH_3$-Mech 1.1. Figure 10(b) shows the oxidation of $CH_4/NH_3/O_2/N_2$ in a alumina flow reactor from the literature [46]. All the mechanisms predicted a similar $NH_3$ consumption trend for methane ammonia co-oxidation in a high-temperature flow reactor, while they all overpredicted CO formation concentration. The NO starting point was captured well, and the NO concentrations were within the prediction range. Thus, the CEU-$NH_3$-Mech 1.1 predicted the flame speed of ammonia-methane well at elevated pressure, and also predicted key intermediate species of ammonia/nitric oxides/methane co-oxidation well.

### 4.5. Sensitivity and kinetic analyses

This part solves three issues: 1) the different effect of methane addition on ignition and flame propagation stages; 2) sensitive reactions comparison for $S_L$ and pressure exponents; 3) the non-monotonic behavior of $\beta$ of the $NH_3/H_2$/air flames. Previous studies have divided the interaction between methane and ammonia chemistries into low and high temperature oxidation. Figure 11(a) presents the reaction pathway of homogeneous ignition simulation of $NH_3/CH_4$/air mixtures with $X_{NH3}$ = 0.6 at 1500 K, one atm and $\phi$ = 1.0, using the present CEU-$NH_3$-Mech 1.1. Arunthanayothin et al. [47] found that at low temperatures, the ammonia addition to methane oxidation depends mainly on the two reactions ($CH_3 + NO_2 = CH_3O + NO$ and $NO + HO_2 = NO_2 + OH$) acting as a catalytic cycle, enhancing the consumption of methane (confirmed in Fig. 11(a)). The $HO_2$ radical is important for low-temperature oxidation of ammonia via reactions: $NH_2 + HO_2 = H_2NO + OH$, and for the enrichment of the $CH_3$, $HO_2$ radical was provided

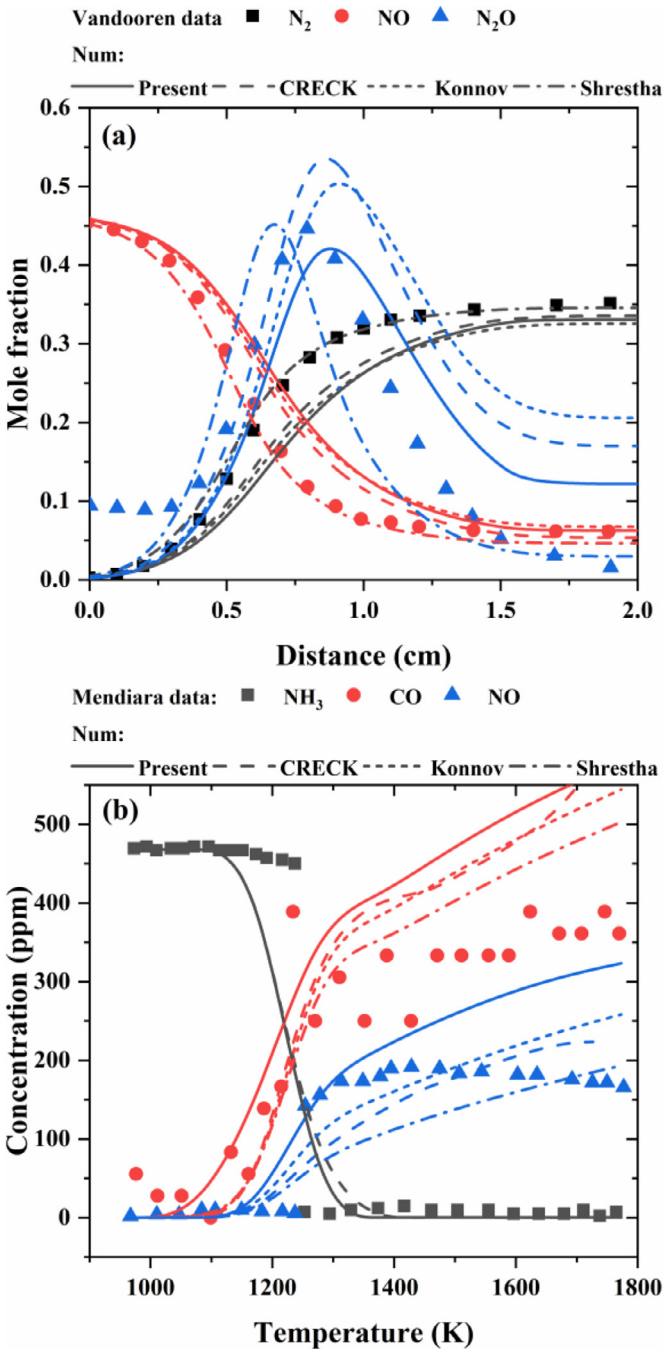


**Fig. 10.** (a) Comparison of experimental data of Vandooren et al. [57] and predictions for oxidation of $NH_3$/NO/Ar in a burner stabilized flame; (b) comparison of experimental data of Mendiara and Glarborg [46] and predictions for oxidation of $CH_4/NH_3/O_2/N_2$ in a alumina flow reactor.

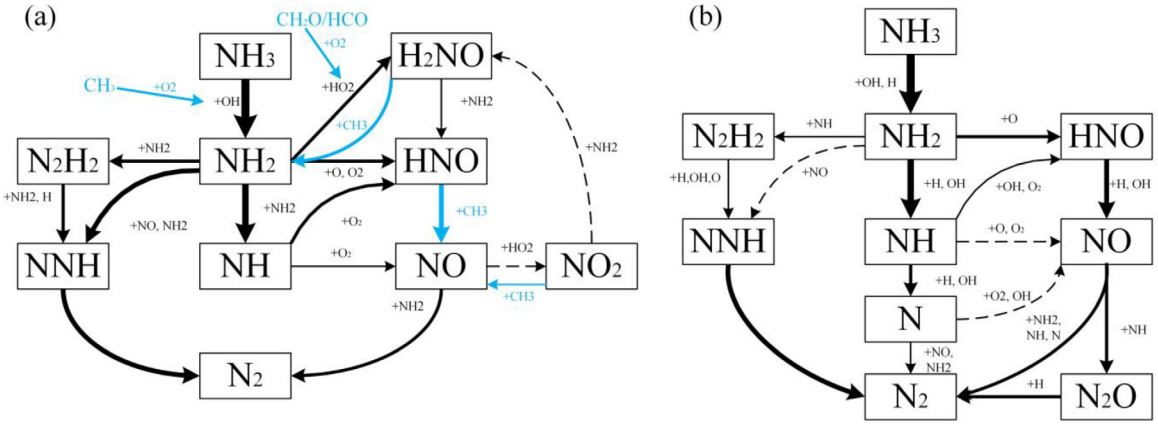


**Fig. 11.** Reaction pathway of $NH_3/CH_4$/air mixtures with $X_{NH3} = 0.6$ at one atm and $\phi = 1.0$ for: (a) ignition delay time simulation at 1500 K in corresponding 1% ammonia conversion; (b) flame speed simulation at the maximum heat release rate in corresponding 1800 K of the reaction zone.

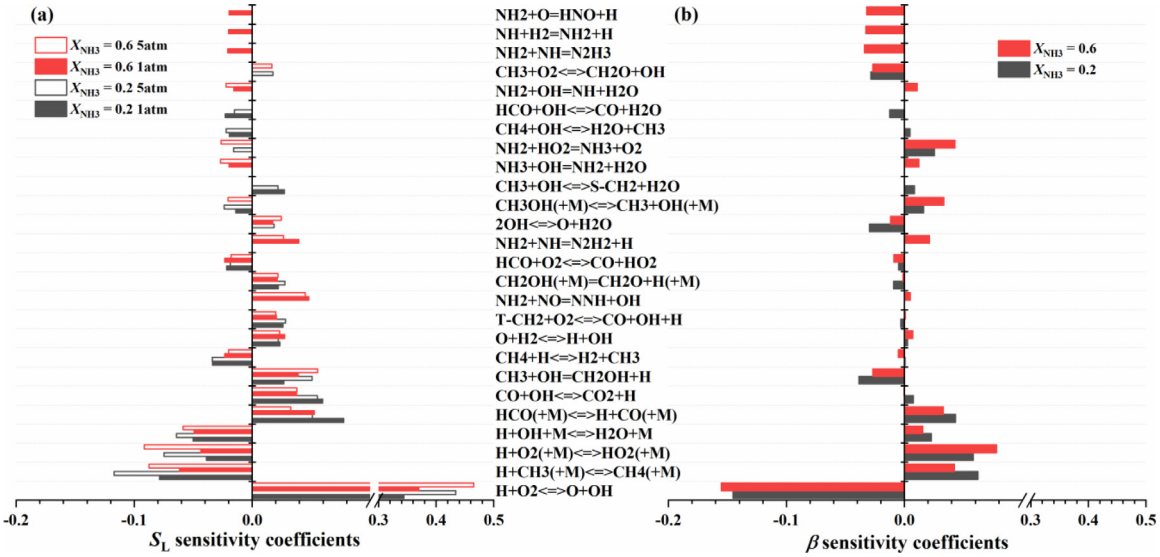


**Fig. 12.** (a) Normalized sensitivity coefficients in predicting $S_L$ of $NH_3/CH_4$/air flames for $X_{NH3} = 0.2$ and 0.4 at one and five atm; (b) sensitivities of the power exponents $\beta$ of $NH_3/CH_4$/air flames.

through $CH_2O/HCO + O_2 = HCO/CO + HO_2$. The $H_2NO$ chemistries are important for both low-temperature oxidation and ignition delay time of $NH_3/CH_4$ (noted by Glarborg et al. [43] and Stagni et al. [48]), were very uncertain and detrimental to simulation accuracy. While confirming the importance of $H_2NO$ chemistry by converting $NH_2$ to HNO, Figure 11(a) also displays the C/N interaction that lies in $HNO + CH_3 = NO + CH_4$, $CH_3 + NO_2 = CH_3O + NO$, and also the $CH_4 + NH_2 = CH_3 + NH_3$ (not shown here). So, at low temperatures, chain propagating reactions of ammonia oxidation and ignition were dominated by $CH_3$ through providing OH: $CH_3 + O_2 = CH_2O + OH$, $CH_3 + O_2 = CH_3O + O$, $CH_3 + HO_2 = OH + CH_3O$ [32].

Figure 11(b) shows flame speed simulation with $X_{NH3} = 0.6$ at the maximum heat release rate location, at high temperatures corresponding to 1800 K in the reaction zone. At this stage, the ammonia conversion ratio reached 90%; large molecules ($CH_3$, $CH_3O$, $HO_2$, $H_2NO$ and $N_2H_2$), which played an active role in low to intermediate temperature ranges in the ignition stage, were all consumed and produced more active small molecules, such as H, O, and OH, dominating the chain propagating reactions. In both the ignition and flame propagation stages, there were three main N-elemental flux whose reaction rate was from fast to slow, such as: 1) $NH_2 \rightarrow NH \rightarrow N_2$; 2) $NH_2 \rightarrow HNO \rightarrow NO \rightarrow N_2$; 3) $NH_2 \rightarrow N_2H_2 \rightarrow NNH \rightarrow N_2$. Compared with Fig. 12(a), the small molecule-dominated N consumption pathway was enhanced, increasing the overall reaction rate, while $H_2NO$ chemistry was omitted and $N_2H_i$ chemistry weakened slightly. This analysis focused on the N-elemental reaction pathway; C-elements were thought to be an additive, and their reaction pathway variations were not developed here. According to the literature, $CH_3O$ chemistry was omitted and the $CH_3$ reacted directly with O to $CH_2O$ [48]. More detailed C/N interaction reactions were investigated by Mendiara and Glarborg [46], Tian et al. [58], and Glarborg et al. [43]; the minor quantities in methane-ammonia co-oxidation were studied experimentally and numerically, and the present reduced C/N interaction from the Konnov mechanism [35] was sufficiently accurate to provide some key species predictions, such as HCN in methane/ammonia flames. For flame speed determination, methane and ammonia chemistries interacted indirectly by sharing the common active radical pool of H, O and OH.

Following is a discussion of the effects of methane content on flame speed and pressure dependence of ammonia/methane mixtures. Figure 12(a) shows normalized sensitivity coefficients in the prediction of $S_L$ of $NH_3/CH_4$/air flames for $X_{NH3} = 0.2$ and 0.6 at one and five atm. The top sensitive reactions with positive signs were $H + O_2 = O + OH$, $OH + H_2 = H_2O + H$ and

$NH_2$ + NO = NNH + OH, and the top sensitive reaction with a negative sign was H + $O_2$ (+ M) = $HO_2$ (+ M). It was found that $H_2$/CO chemistries still dominated the high-temperature oxidation of $NH_3/CH_4$ (*i.e.*, flame speed determination, at low ammonia content). $CH_3$, $CH_2OH$, and HCO radicals significantly affected flame speeds; while at high ammonia content, the $NH_2$ + NO, $NH_2$ + O, and $NH_2$ + H–as well as the $NH_2$ + NH–determined the flux direction of N-elements and the flame speed. In addition to the most important chain-branching reactions of $NH_2$ + NO = NNH +OH/ $N_2$ + $H_2O$ and $NH_2$ + $HO_2$ = $H_2NO$ + OH/ $NH_3$ + $O_2$ (important for both NO formation and $S_L$ predicting), $N_2H_i$ chemistries with high uncertainty were thought to be key determinants of flame speed, especially in rich equivalence ratios and elevated pressures, through $NH_i$ recombination reactions [25]. They were similar to $CH_3$ recombination reactions to form $C_2H_i$; the formed $N_2H_i$ finally reacted to NNH and $N_2$. The three-body termination reactions of $CH_3$ to $CH_4$ retarded flame propagation, even in high ammonia content flames. Almost all reactions' sensitivities were enhanced as pressure increased from one to five atm, except several $NH_2$ reactions on the top of the chart. Some reactions were only important at elevated pressures, like $NH_2$ + $HO_2$ = $NH_3$ + $O_2$, which slowed the overall reaction rate because more $HO_2$ radicals were formed through the three body termination reactions H + $O_2$ (+M) = $HO_2$ (+ M) at elevated pressures. Based on reaction pathway and sensitivity analyses, a more accurate estimation of $NH_2$ + O = HNO + H became a critical milestone in the ammonia mechanism; it also boosted production of NO at intermediate and high temperatures in the flow reactor, as noted by Glarborg et al.[43], Stagni et al. [48]. The only theoretical calculations of rate constants, by Bozzelli and Dean [59] and Sumathi et al. [60] differed by 1.4 times at 1000–2000 K. Thus, modification of the present mechanism improved its flame speed prediction performance, as well as its description of the high temperature ammonia oxidation process.

Like the sensitivity of laminar burning velocity, the sensitivity of coefficients with respect to the rate constant k, can be defined as [61]:

$$Sens(\beta,\ k) = \frac{\partial \beta}{\partial k}\frac{k}{\beta} = \frac{Sens(S_L,\ k) - Sens(S_{L0},\ k)}{\beta \cdot ln\frac{P}{P_0}} \quad (3)$$

where $S_L$ and $S_{L0}$ are laminar burning velocities at $P$ and $P_0$. However, the sensitivity coefficients of pressure exponents $\beta$, shown in Fig. 12(b), differed from $S_L$, even though some reactions which are important for burning velocity predictions, did not affect the calculated $\beta$ coefficients. For instance, reaction CO + OH = $CO_2$ + H, which ranks in the top ten in all $NH_3/CH_4$/air flames, was not sensitive to pressure dependence. The same consideration was applicable to reaction $NH_2$ + NO = NNH + OH, $CH_4$ + H = $CH_3$ + $H_2$. As a result, modification of the rate constants of these reactions influenced calculated burning velocities, without a noticeable change in calculated power exponents, $\beta$. However, $\beta$ were more sensitive to reactions like the $NH_2$ + NH = $N_2H_3$, $NH_2$ + H = NH + $H_2$, $NH_2$ + O = HNO + H and $NH_2$ + $HO_2$ = $NH_3$ + $O_2$ than $S_L$ to these reactions, so high-pressure ammonia flame speed was more difficult to predict accurately than high-pressure methane flame, due to the uncertainties of these sensitive reactions, confirming that $\beta$ may serve as a useful target for model validation and improvement.

To explain the unusual behavior of $NH_3/H_2$/air flames with a minimum of pressure exponents $\beta$ for $NH_3$ mole fraction around 0.5 (shown in Fig. 6), a sensitivity analysis of $S_L$ of $NH_3/H_2$/air flames with $X_{NH3}$ from zero to one at one and five atm was performed (Fig. 13). Among the $NH_3/H_2$/air flames, the maximum sensitivity of almost all reactions occurred for flames with values of $X_{NH3}$ between 0.4 and 0.6–especially the three important chain-terminating reactions– H + $O_2$ (+ M) = $HO_2$ (+ M), H + OH +M = $H_2O$ + M and $NH_2$ + NH = $N_2H_3$. The same can

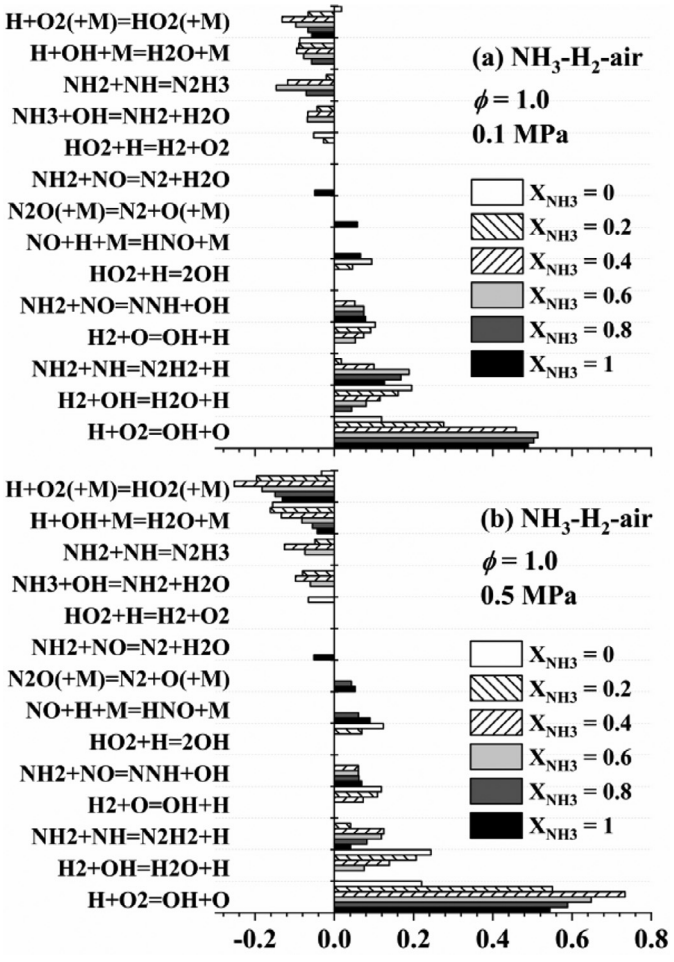


**Fig. 13.** Normalized sensitivity coefficients in prediction of $S_L$ of $NH_3/H_2$/air flames for $X_{NH3}$ = 0 - 1 at 1 and 5 atm.

be applied to positive chain branching and propagating reactions H + $O_2$ = O + OH and $NH_2$ + NH = $N_2H_2$ + H. Not only, the sensitivity coefficients of $S_L$ at medium $X_{NH3}$ contents get maximum, as shown in Fig. 13, but also the variation magnitude of the sensitivity coefficients of $S_L$ from 1 to 5 atm at medium $X_{NH3}$ get maximum. This means $S_L$ variation is most sensitive to these pressure-sensitive reactions at medium $X_{NH3}$ conditions. The reaction rates of the four top sensitive reactions are integrated along the reaction distance axis separately to obtain the integrated reaction rate, $S$. Figure 14(a) shows that as $X_{NH3}$ increases, the reaction rates of H + $O_2$ branching reactions decrease; while the reaction rates of $NH_2$ + NH branching reactions get maximum at $X_{NH3}$ = 0.2–0.6. Figure 14(b) shows the integrated reaction rate ratio from 1 to 5 atm. It is found that top sensitive reactions like the three-body termination and $NH_i$ combination reactions have minimum enhancement at medium $X_{NH3}$ contents which is totally similar to the variation trend of pressure exponents, $\beta$. This reaction has been proved to be the dominant reason for the varying pressure dependence of LBV of $H_2$/air mixtures [51,52]. This means at medium ammonia content, the enhancement of reactivity by pressure increase has a minimum.

### 4.6. Over-rich behavior of $NH_3/CH_4$/air flames

Figure 7(a) shows that the pressure power exponents of $NH_3/CH_4$/air flames at $X_{NH3}$ = 0.2 displayed obvious non-monotonic behavior at rich equivalence ratios. At the same time, in Fig. 7(b), these turning points did not appear at $X_{NH3}$ = 0.6 con-

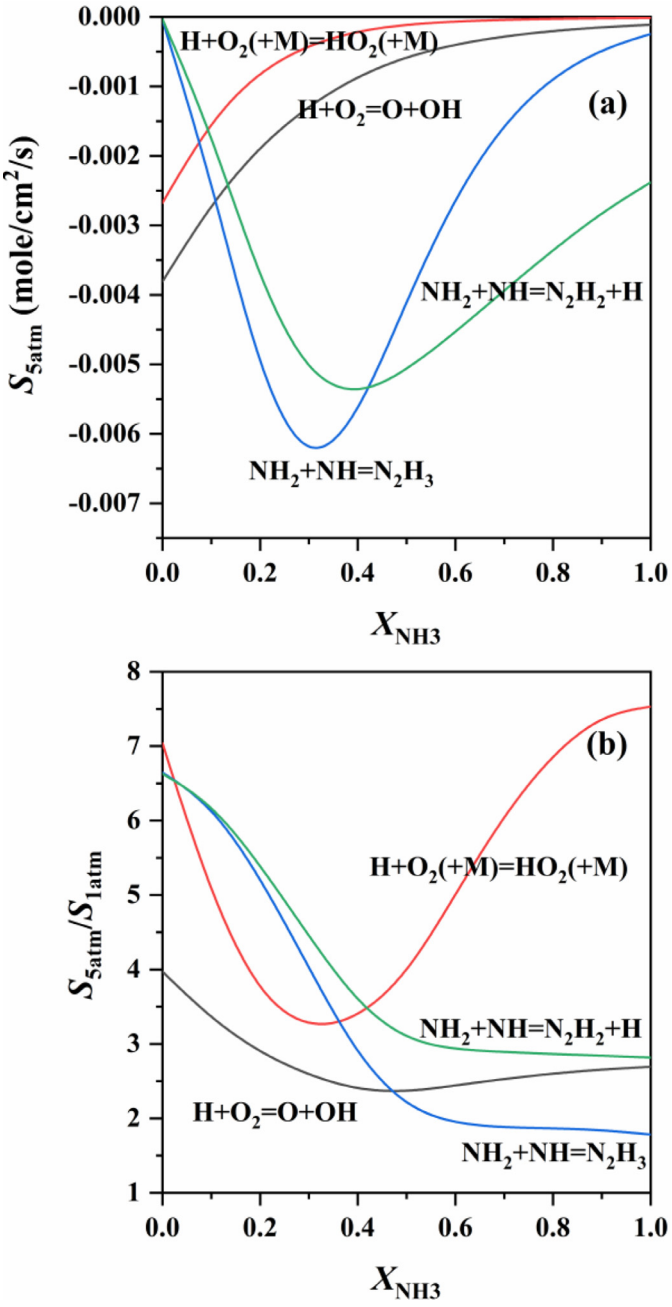


**Fig. 14.** (a) Integrated reaction rates of top sensitive reactions to $S_L$ at 5 atm; (b) the ratio of integrated reaction rates from 1 to 5 atm.

ditions which means increasing ammonia content changes the rich flame chemistry. Figure 15 shows that major species mole fraction and adiabatic flame temperature of $NH_3/CH_4$/air flames along the reaction zone distance for $X_{NH3}$ = 0.2 and 0.6 at one atm at $\phi$ from stoichiometric, to slightly-rich, then to over-rich conditions. It was found that at $\phi$ = 1.0, the major species in the reaction zone in cases (a) and (d) shared the same trend, *i.e.*, $NH_3$ and $CH_4$ are fully consumed in the reaction zone, via the intermediate products CO and $H_2$ and formed $H_2O$ and $CO_2$. When the equivalence ratio increased to 1.3, the same is applied to case (b); while in case (e), the peak $H_2O$ concentration is higher than the final equilibrium concentration, so does the $CO_2$; at the same time, $H_2$ and CO concentration keeps increasing along with the reaction axis distance. As the equivalence ratio further increased to 1.6, for both cases (c)(f), the $H_2O$, $CO_2$ now began to decompose in the post-flame zone through reverse reactions of OH + $H_2$ = H + $H_2O$ and CO + OH = $CO_2$ + H, accompanied by the increase of $H_2$, CO concentration which is also confirmed in [54,62]. These two reverse reactions are endothermic and lead to the decrease of the flame temperature at the post-flame zone, thus, the peak flame temperature was higher than the final adiabatic flame temperatures (referred to as the SAFT (super-adiabatic-flame-temperature) phenomenon) [63,64]. It is found that the increase of $H_2$ and CO in cases (c)(f) is more obvious than the decreasing $H_2O$ and $CO_2$, which is because the unburnt $NH_3$ and $CH_4$ in the post-flame zone slowly oxidized and produced extra $H_2$ and CO; for the O-elemental flux balance, the extra OH radicals eventually reacted with the unburnt $NH_3$ and CO producing $H_2O$ and $CO_2$ via $NH_3$ + OH = $NH_2$ + $H_2O$ and CO + OH = $CO_2$ + H.

Figure 16 shows the H elemental-flux in the reaction zone and post-flame zone of $NH_3/CH_4$/air flames for $X_{NH3}$ = 0.2 and 0.6 at one atm corresponding to cases (b)(e) in Fig. 15. The reaction zone is defined as the maximum gradient location of the temperature profile, *i.e.*, the flame front and the post-flame zone is 1 cm downstream of the flame front location. The percentages in the figure are the conversion ratio of ammonia and methane at that location, red-marked radicals and species are O elemental-flux participated in the H radical conversion process. The major producing and consuming reactions for hydrogen in the reaction zone were similar for both low and high ammonia content shown in Fig. 16(a) and (c), except that the hydrogen comes from $NH_2$ and $CH_2O$ in different proportions. Considering the O-elemental balance, all the red-marked OH and NO radicals are eventually converted to $H_2O$ as shown in the figure. As the flame propagates downstream and approaches the equilibrium state (shown in cases (b) (d)), due to the faster reaction process in low ammonia content case (d), the conversion ratio of fuel is always higher than case (b). The reaction pathway analysis validated our assumption above that at high ammonia content conditions, $H_2O$ reacted with abundant H radical and went back to the $H_2$. However, in the low ammonia content flame (case (d)), the H radical pool is not as saturated as in case (b), $H_2$ + OH = $H_2O$ + H conversion still retains going forwardly. It could be expected as the equivalence ratio further increases, even for the low-ammonia-content flames, the $H_2O \rightarrow H_2$ conversion happens, as can be seen in Fig. 15(c). For the high ammonia content Fig. 15(f), the decrease of flame temperature and the increased concentration of $H_2$ were more obvious than in case Fig. 15(c). Thus, increasing the ammonia content in the fuel mixture advances the transition from “moderately-rich flame chemistry” to “over-rich flame chemistry”.

Goswami et al. [65] and Wang et al. [30] has attributed the non-monotonic behavior of $\beta$ to the competition of reaction $CH_3$ + $CH_3$ = $C_2H_6$ dominating in very rich flames with reaction $CH_3$ + H + M = $CH_4$ acting as major radical consumption mechanism elsewhere, as suggested by Seshadri et al. [66] in their asymptotic analysis. Figure 17 shows the consumption percentage of H radical via different reactions for $X_{NH3}$ = 0.2 and 0.6, $\phi$ = 1.3 at one atm. At slightly rich equivalence ratios ($\phi$ = 1.0 - 1.3), $CH_3$ + H (+M) = $CH_4$ (+M) competed with H + $O_2$ = O + OH in consuming H radicals and led to the decrease of laminar burning velocity. The former three-body termination reaction was favored at elevated pressures, leading to decreasing pressure coefficients. While as $\phi$ increased further ($\phi$ = 1.3 - 1.6), the $CH_3$ + $CH_3$ (+M) = $C_2H_6$ (+M) began to consume a large proportion of $CH_3$, relieving the competition between the chain-branching reaction H + $O_2$. The flame chemistry transited to C2 radicals, dominated through $C_2H_n(\rightarrow CH_2CO)\rightarrow HCCO\rightarrow CO$, and led to the increase of pressure exponents. Figure 18 also displays the oxidation pathway of $NH_3/CH_4$/air flames for $X_{NH3}$ = 0.2 and 0.6, $\phi$ = 1.3 at one atm. At moderate rich conditions, $C_2H_n$ chemistry and $N_2H_n$ chemistry were important in the chain propagating

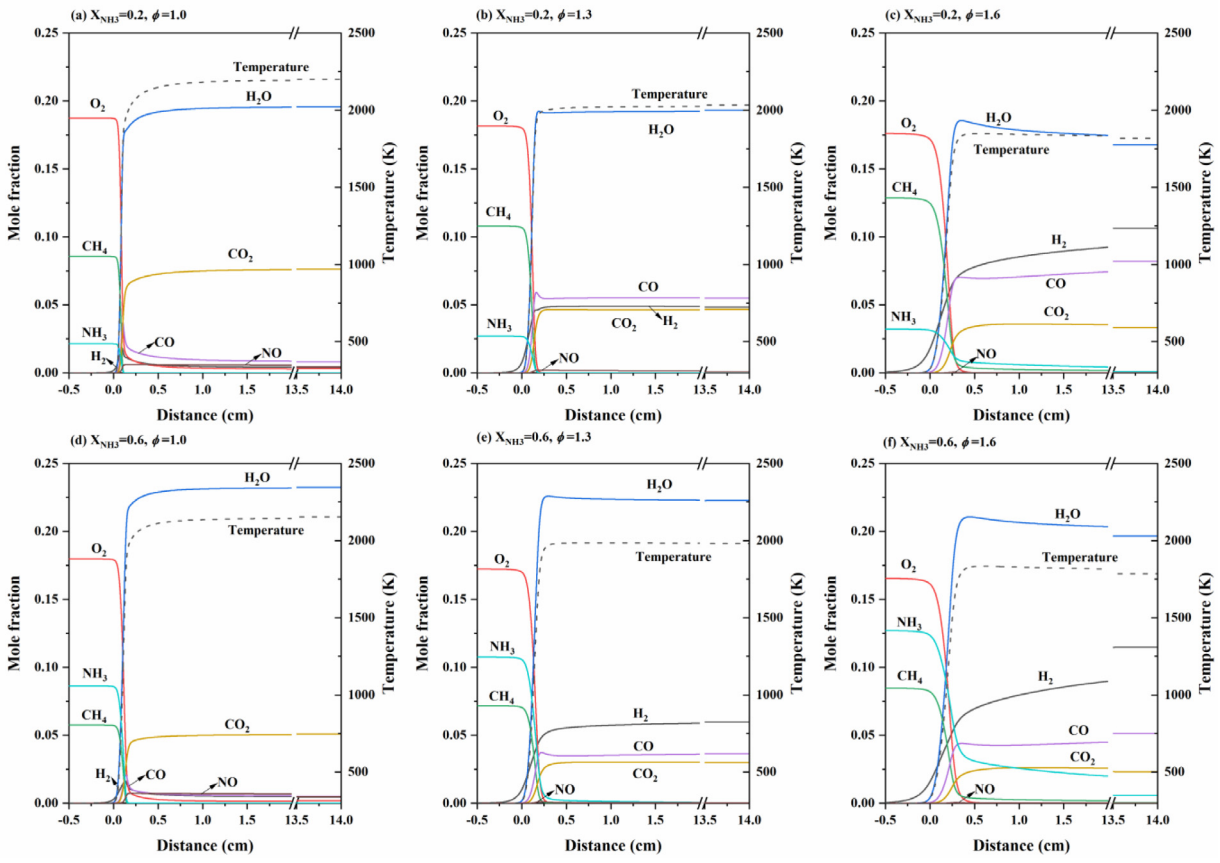


**Fig. 15.** Major species mole fraction, adiabatic flame temperature and reaction pathway of $NH_3/CH_4$/air flames along the reaction zone distance for $X_{NH3}$ = 0.2 and 0.6 at one atm.

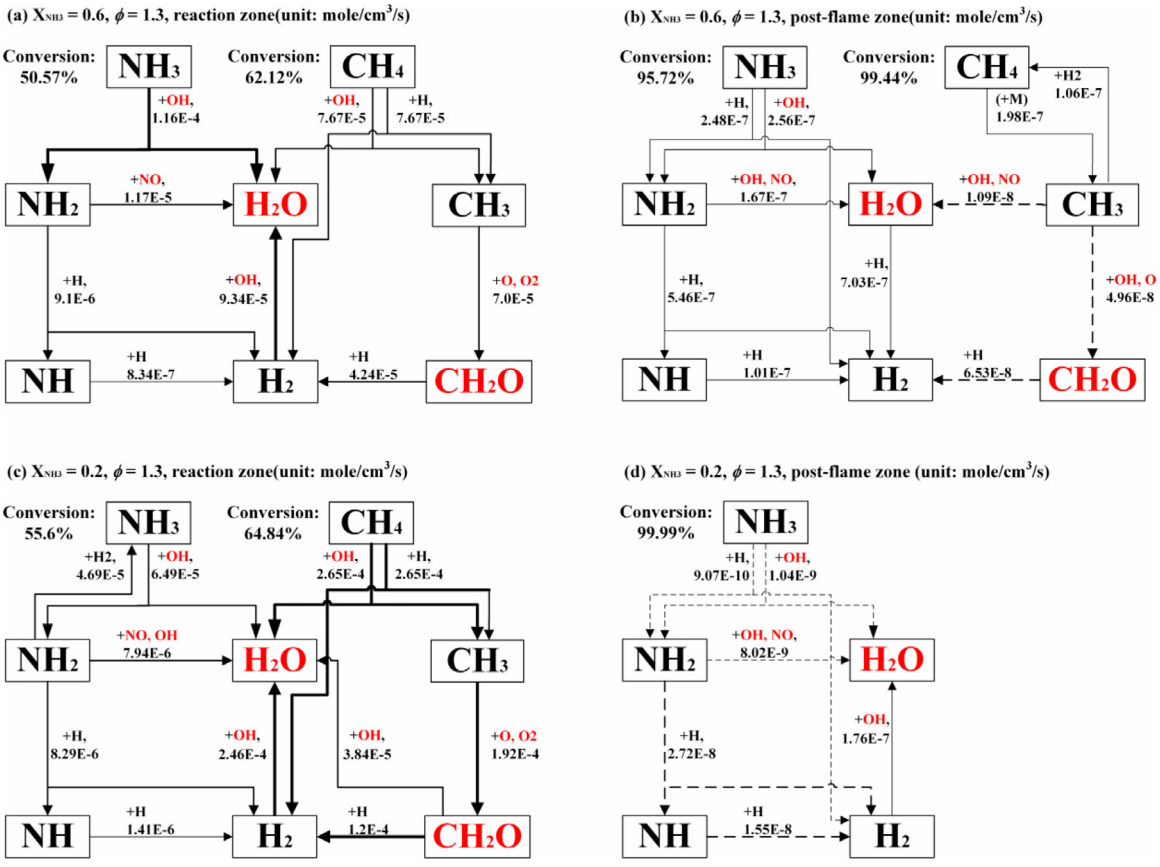


**Fig. 16.** H elemental-flux in the reaction zone (maximum gradient location of the temperature profile) and post-flame zone (1 cm downstream of the flame front) of $NH_3/CH_4$/air flames for $X_{NH3}$ = 0.2 and 0.6 at one atm (thickness represents the reaction flux magnitude).

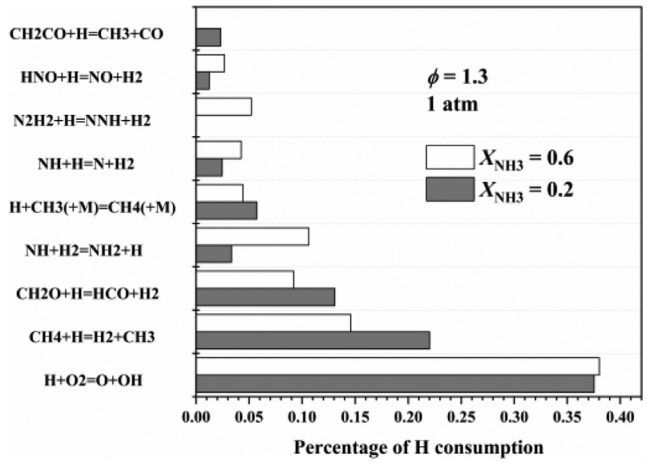


**Fig. 17.** Consumption percentage of H radical through different reactions for $X_{NH3}$ = 0.2 and 0.6, $\phi$ = 1.3 at one atm.

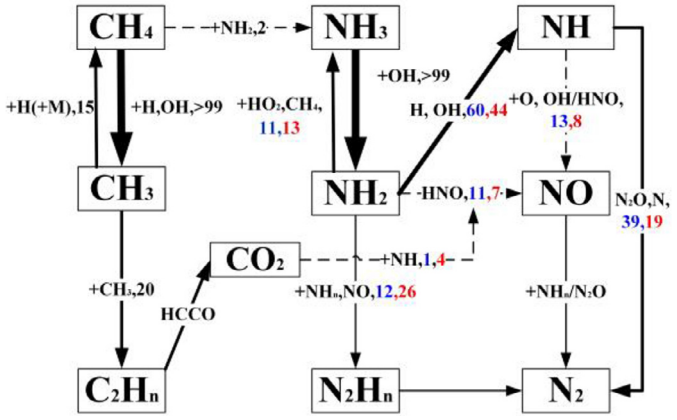


**Fig. 18.** Oxidation pathway of $NH_3/CH_4$/air flames for $X_{NH3}$ = 0.2 and 0.6, $\phi$ = 1.3 at one atm. (Numbers are percentage of consumption of N or C-elements for $X_{NH3}$ = 0.2 and 0.6 separately).

reactions. A strong retarding reaction existed from $CH_3$ + H (+M) = $CH_4$ (+M) for H radical consumption. Comparable reaction from $NH_2$ to $NH_3$: $NH_2$ + $HO_2$ = $NH_3$ + $O_2$ was not as retarding as $CH_3$ + H (+M) = $CH_4$ (+M) according to the sensitivity coefficients shown in Fig. 13(a); it mainly consumed the $HO_2$ radical, rather than the more active H radicals and its consumption percentage for $HO_2$ was also lower than the consumption percentage for H of $CH_3$ + H (+M) = $CH_4$ (+M), so its retarding role was weaker. The consumption proportions of C-elements were the same in both low and high ammonia content; while for N-elements, as $X_{NH3}$ increased, more $N_2H_n$ formed through $NH_2$ recombination reactions. Abundant $NH_2$ radicals promoted the reaction $NH_2$ + O = HNO + H, which provided H radicals, followed by the reaction HNO + H = NO + $H_2$, leading to the hydrogen concentration increase in Fig. 15(e).

Another HNO formation route (NH + $CO_2$ = HNO + CO) converted $CO_2$ into CO, leading to the concentration variation in Fig. 15(e). Until now, it was understood why non-monotonic behavior of $\beta$ (Fig. 8(a)) disappeared in high ammonia content conditions in Fig. 8(b): (1) $NH_2$ played a more important role than $CH_3$, so the retarding action of $CH_3$ + H (+M) = $CH_4$ (+M) was weakened, and as the pressure increased, H radicals consumption occurred mainly through $N_2H_n$ chemistry, not three-body termination reactions. (2) $N_2H_n$ and $H_2O$ decomposed to produce $H_2$, simultaneously; $C_2H_n$ and $CO_2$ decomposed to produce CO, extra O atoms go back to $H_2O$ and $CO_2$, and this transition occurred at lower equivalence ratios for higher ammonia content flames. (3) Flame temperature decreased and super adiabatic flame temperature occurred; the entire flame chemistry transit to $N_2H_n$ domination, and the abundant unburned hydrogen made possible the rich-quench-lean stage combustion of ammonia (Eqs. (1)–(3)).

## 5. Conclusions

The main conclusions from this work are as follows:

1. Measured $S_L$ data for $NH_3/CH_4$/air and $NH_3/H_2$/air flames at elevated pressures were in excellent agreement with the data in the literature; however, previous data were scarce. For stoichiometric conditions, prediction accuracy was greatly affected by hydrocarbon and hydrogen chemistry, and for the wide range of equivalence ratios, ammonia chemistry played an important role. The CEU-$NH_3$ 1.1 mechanism was successfully validated against the flame speed of $NH_3/CH_4$/air and $NH_3$/syngas/air in a wide range of equivalence ratios and elevated pressures. The high-pressure $S_L$ data at medium ammonia content diverged significantly among the different mechanisms, and it was a better test of the mechanism's accuracy.
2. The empirical power law pressure described the pressure dependence of the $S_L$ of $NH_3/CH_4$/air; pressure exponents $\beta$ of the $NH_3/H_2$/air flames first decreased and then increased with increased $X_{NH3}$, which is due to the top sensitive reactions like the three-body termination and $NH_i$ combination reactions have minimum enhancement at medium $X_{NH3}$ contents.
3. The present mechanism was validated against oxygen-enriched ammonia-oxygen-diluent flame speeds and ignition delay time of ammonia-methane; it was found that the oxygen-enriched conditions increased prediction uncertainty in ammonia chemistries from different mechanisms. The present mechanism offers reliable predictions for intermediate species formation in high temperature methane/ammonia co-oxidation.
4. Using the present mechanism, sensitivity and kinetic analyses were conducted for low and high temperature oxidation of ammonia with the addition of methane. It was found that $CH_3$ was important for low temperature IDT by enhancing $CH_3O$ and $H_2NO$; the reaction rate of $NH_2$ + O = HNO + H must be reevaluated for its importance in high-temperature ammonia oxidation.
5. The sensitivity analysis of pressure coefficients $\beta$ confirms its different independence compared to $S_L$, and serves as a validation parameter for kinetic mechanisms. The non-monotonic behavior of $NH_3/CH_4$/air flames at rich equivalence ratios occurred because of the competition between $CH_3$ and $N_2H_i$ chemistries, increasing the ammonia content advances the occurrence of super-adiabatic flame temperature at lower equivalence ratio conditions by enriching the H radical pool and converting $H_2O$ back to $H_2$ in the post-flame zone. High CO and $H_2$ formation from $CO_2$ and $H_2O$ in the post-flame zone of $NH_3/CH_4$/air are promising for the ammonia' RQL (rich-quench-lean) combustion.

## Declaration of Competing Interest

The authors declare that they have no known competing financial interests or personal relationships that could have appeared to influence the work reported in this paper.

## Acknowledgements

This work was supported by Fundamental Research Funds for the Central Universities (2021FZZX001–11), National Natural Science Foundation of China (52125605), the State Key Laboratory of

Clean Energy Utilization (ZJUCEU2019001) and King Abdullah University of Science and Technology.

## Supplementary materials

Supplementary material associated with this article can be found, in the online version, at doi:10.1016/j.combustflame.2021.111788.

## References


[1] IEAGlobal energy review 2021, International Energy Agency, 2021.
[2] A. Valera-Medina, H. Xiao, M. Owen-Jones, W.I.F. David, P.J. Bowen, Ammonia for power, Prog. Energy Combust. Sci. 69 (2018) 63–102.
[3] H. Kobayashi, A. Hayakawa, K.D.K.A. Somarathne, E.C. Okafor, Science and technology of ammonia combustion, Proc. Combust. Inst. 37 (2019) 109–133.
[4] S. Frigo, R. Gentili, Analysis of the behaviour of a 4-stroke Si engine fuelled with ammonia and hydrogen, Int. J. Hydrog. Energy 38 (2013) 1607–1615.
[5] O. Kurata, N. Iki, T. Matsunuma, T. Inoue, T. Tsujimura, H. Furutani, H. Kobayashi, A. Hayakawa, Performances and emission characteristics of $NH_3$-air and $NH_3$-$CH_4$-air combustion gas-turbine power generations, Proc. Combust. Inst. 36 (2017) 3351–3359.
[6] A. Hayakawa, T. Goto, R. Mimoto, Y. Arakawa, T. Kudo, H. Kobayashi, Laminar burning velocity and Markstein length of ammonia/air premixed flames at various pressures, Fuel 159 (2015) 98–106.
[7] O. Mathieu, E.L. Petersen, Experimental and modeling study on the high-temperature oxidation of Ammonia and related $NO_x$ chemistry, Combust. Flame 162 (2015) 554–570.
[8] A. Valera-Medina, R. Marsh, J. Runyon, D. Pugh, P. Beasley, T. Hughes, P. Bowen, Ammonia–methane combustion in tangential swirl burners for gas turbine power generation, Appl. Energy 185 (2017) 1362–1371.
[9] C.F. Ramos, R.C. Rocha, P.M.R. Oliveira, M. Costa, X.S. Bai, Experimental and kinetic modelling investigation on NO, CO and $NH_3$ emissions from $NH_3$/$CH_4$/air premixed flames, Fuel 254 (2019) 115693.
[10] E.C. Okafor, K.D.K.A. Somarathne, R. Ratthanan, A. Hayakawa, T. Kudo, O. Kurata, N. Iki, T. Tsujimura, H. Furutani, H. Kobayashi, Control of $NO_x$ and other emissions in micro gas turbine combustors fuelled with mixtures of methane and ammonia, Combust. Flame 211 (2020) 406–416.
[11] R.C. Rocha, C.F. Ramos, M. Costa, X.S. Bai, Combustion of $NH_3$/$CH_4$/Air and $NH_3$/$H_2$/air mixtures in a porous burner: experiments and kinetic modeling, Energy Fuels 33 (2019) 12767–12780.
[12] A.A. Konnov, A. Mohammad, V.R. Kishore, N.I. Kim, C. Prathap, S. Kumar, A comprehensive review of measurements and data analysis of laminar burning velocities for various fuel+air mixtures, Prog. Energy Combust. Sci. 68 (2018) 197–267.
[13] K. Takizawa, A. Takahashi, K. Tokuhashi, S. Kondo, A. Sekiya, Burning velocity measurements of nitrogen-containing compounds, J. Hazard. Mater. 155 (2008) 144–152.
[14] P.D. Ronney, Effect of chemistry and transport properties on near-limit flames at microgravity, Combust. Sci. Technol. 59 (1988) 123–141.
[15] U.J. Pfahl, M.C. Ross, J.E. Shepherd, K.O. Pasamehmetoglu, C. Unal, Flammability limits, ignition energy, and flame speeds in $H_2$–$CH_4$–$NH_3$–$N_2O$–$O_2$–$N_2$ mixtures, Combust. Flame 123 (2000) 140–158.
[16] T. Jabbour, D.F. Clodic, J. Terry, S. Kondo, Burning velocity and refrigerant flammability classification, ASHRAE Trans. (2004) 522–533.
[17] P. Kumar, T.R. Meyer, Experimental and modeling study of chemical-kinetics mechanisms for $H_2$-$NH_3$-air mixtures in laminar premixed jet flames, Fuel 108 (2013) 166–176.
[18] J. Li, H. Huang, N. Kobayashi, Z. He, Y. Nagai, Study on using hydrogen and ammonia as fuels: combustion characteristics and $NO_x$ formation, Int. J. Energy Res. 38 (2014) 1214–1223.
[19] A. Ichikawa, A. Hayakawa, Y. Kitagawa, K.K.A. Somarathne, T. Kudo, H. Kobayashi, Laminar burning velocity and Markstein length of ammonia/hydrogen/air premixed flames at elevated pressures, Int. J. Hydrog. Energy 40 (2015) 9570–9578.
[20] J.H. Lee, J.H. Kim, J.H. Park, O.C. Kwon, Studies on properties of laminar premixed hydrogen-added ammonia/air flames for hydrogen production, Int. J. Hydrog. Energy 35 (2010) 1054–1064.
[21] C. Lhuillier, P. Brequigny, N. Lamoureux, F. Contino, C. Mounaïm-Rousselle, Experimental investigation on laminar burning velocities of ammonia/hydrogen/air mixtures at elevated temperatures, Fuel 263 (2020) 116653.
[22] X. Han, Z. Wang, M. Costa, Z. Sun, Y. He, K. Cen, Experimental and kinetic modeling study of laminar burning velocities of $NH_3$/air, $NH_3$/$H_2$/air, $NH_3$/CO/air and $NH_3$/$CH_4$/air premixed flames, Combust. Flame 206 (2019) 214–226.
[23] E.C. Okafor, Y. Naito, S. Colson, A. Ichikawa, T. Kudo, A. Hayakawa, H. Kobayashi, Experimental and numerical study of the laminar burning velocity of $CH_4$-$NH_3$-air premixed flames, Combust. Flame 187 (2018) 185–198.
[24] X. Han, Z. Wang, Y. He, Y. Zhu, K. Cen, Experimental and kinetic modeling study of laminar burning velocities of $NH_3$/syngas/air premixed flames, Combust. Flame 213 (2020) 1–13.
[25] S. Wang, Z. Wang, A.M. Elbaz, X. Han, Y. He, M. Costa, A.A. Konnov, W.L. Roberts, Experimental study and kinetic analysis of the laminar burning velocity of $NH_3$/syngas/air, $NH_3$/CO/air and $NH_3$/$H_2$/air premixed flames at elevated pressures, Combust. Flame 221 (2020) 270–287.
[26] E.C. Okafor, Y. Naito, S. Colson, A. Ichikawa, T. Kudo, A. Hayakawa, H.J.C. Kobayashi, Flame, Measurement and modelling of the laminar burning velocity of methane-ammonia-air flames at high pressures using a reduced reaction mechanism, Combust. Flame 204 (2019) 162–175.
[27] R.P. Lindstedt, F.C. Lockwood, M.A. Selim, Detailed kinetic modelling of chemistry and temperature effects on ammonia oxidation, Combust. Sci. Technol. 99 (1994) 253–276.
[28] J.A. Miller, M.D. Smooke, R.M. Green, R.J. Kee, Kinetic modeling of the oxidation of ammonia in flames, Combust. Sci. Technol. 34 (1983) 149–176.
[29] G.P. Smith, D.M. Golden, M. Frenklach, N.W. Moriarty, B. Eiteneer, M. Goldenberg, C.T. Bowman, R.K. Hanson, S. Song, W.C. Gardiner Jr, V.V. Lissianski, Z. Qin, http://www.me.berkeley.edu/gri_mech/, (2011).
[30] S. Wang, Z. Wang, Y. He, X. Han, Z. Sun, Y. Zhu, M. Costa, Laminar burning velocities of $CH_4$/$O_2$/$N_2$ and oxygen-enriched $CH_4$/$O_2$/$CO_2$ flames at elevated pressures measured using the heat flux method, Fuel 259 (2020) 116152.
[31] S. Wang, Z. Wang, X. Han, C. Chen, Y. He, Y. Zhu, K. Cen, Experimental and numerical study of the effect of elevated pressure on laminar burning velocity of lean $H_2$/CO/$O_2$/diluents flames, Fuel 273 (2020) 117753.
[32] H. Xiao, S. Lai, A. Valera-Medina, J. Li, J. Liu, H. Fu, Experimental and modeling study on ignition delay of ammonia/methane fuels, 44 (2020) 6939–6949.
[33] B. Mei, X. Zhang, S. Ma, M. Cui, H. Guo, Z. Cao, Y. Li, Experimental and kinetic modeling investigation on the laminar flame propagation of ammonia under oxygen enrichment and elevated pressure conditions, Combust. Flame 210 (2019) 236–246.
[34] Z. Wang, X. Han, Y. He, R. Zhu, Y. Zhu, Z. Zhou, K. Cen, Experimental and kinetic study on the laminar burning velocities of $NH_3$ mixing with $CH_3OH$ and $C_2H_5OH$ in premixed flames, Combust. Flame 229 (2021) 111392.
[35] G. Capriolo, C. Brackmann, M. Lubrano Lavadera, T. Methling, A.A. Konnov, An experimental and kinetic modeling study on nitric oxide formation in premixed C3 alcohols flames, Proc. Combust. Inst. 38 (2020) 805–812.
[36] K.J. Bosschaart, L.P.H. de Goey, The laminar burning velocity of flames propagating in mixtures of hydrocarbons and air measured with the heat flux method, Combust. Flame 136 (2004) 261–269.
[37] K.J. Bosschaart, L.P.H. de Goey, Detailed analysis of the heat flux method for measuring burning velocities, Combust. Flame 132 (2003) 170–180.
[38] L.P.H. De Goey, A. Van Maaren, R.M. Quax, Stabilization of adiabatic premixed laminar flames on a flat flame burner, Combust. Sci. Technol. 92 (1993) 201–207.
[39] T. Varga, C. Olm, T. Nagy, I.G. Zsély, É. Valkó, R. Pálvölgyi, H.J. Curran, T. Turányi, Development of a joint hydrogen and syngas combustion mechanism based on an optimization approach, 48 (2016) 407–422.
[40] "Chemical-kinetic mechanisms for combustion applications", Mechanical and Aerospace Engineering (Combustion Research), University of California at San Diego. http://web.eng.ucsd.edu/mae/groups/combustion/mechanism.html.
[41] S. Inomata, N. Washida, Rate constants for the reactions of $NH_2$ and HNO with atomic oxygen at temperatures between 242 and 473K, J. Phys. Chem. A 103 (1999) 5023–5031.
[42] K.P. Shrestha, C. Lhuillier, A.A. Barbosa, P. Brequigny, F. Contino, C. Mounaïm-Rousselle, L. Seidel, F. Mauss, An experimental and modeling study of ammonia with enriched oxygen content and ammonia/hydrogen laminar flame speed at elevated pressure and temperature, Proc. Combust. Inst. 38 (2021) 2163–2174.
[43] P. Glarborg, J.A. Miller, B. Ruscic, S.J. Klippenstein, Modeling nitrogen chemistry in combustion, Prog. Energy Combut. Sci. 67 (2018) 31–68.
[44] D.L. Baulch, C.T. Bowman, C.J. Cobos, R.A. Cox, T. Just, J.A. Kerr, M.J. Pilling, D. Stocker, J. Troe, W. Tsang, R.W. Walker, J. Warnatz, Evaluated kinetic data for combustion modeling: supplement II, 34 (2005) 757–1397.
[45] P. Brequigny, F. Halter, C. Mounaïm-Rousselle, Lewis number and Markstein length effects on turbulent expanding flames in a spherical vessel, Exp. Therm. Fluid Sci. 73 (2016) 33–41.
[46] T. Mendiara, P. Glarborg, Ammonia chemistry in oxy-fuel combustion of methane, Combust. Flame 156 (2009) 1937–1949.
[47] S. Arunthanayothin, A. Stagni, Y. Song, O. Herbinet, T. Faravelli, F. Battin-Leclerc, Ammonia–methane interaction in jet-stirred and flow reactors: an experimental and kinetic modeling study, Proc. Combust. Inst. 38 (2021) 345–353.
[48] A. Stagni, C. Cavallotti, S. Arunthanayothin, Y. Song, O. Herbinet, F. Battin-Leclerc, T. Faravelli, An experimental, theoretical and kinetic-modeling study of the gas-phase oxidation of ammonia, React. Chem. Eng. 5 (2020) 696–711.
[49] CHEMKIN, Pro. "R2, ANSYS." Inc., San Diego, (2019).
[50] L.P.H. De Goey, L.M.T. Somers, W.M.M.L. Bosch, R.M.M. Mallens, Modeling of the small scale structure of flat burner-stabilized flames, Combust. Sci. Technol. 104 (1995) 387–400.
[51] M.P. Burke, M. Chaos, F.L. Dryer, Y. Ju, Negative pressure dependence of mass burning rates of $H_2$/CO/$O_2$/diluent flames at low flame temperatures, Combust. Flame 157 (2010) 618–631.
[52] M. Goswami, J.G.H. van Griensven, R.J.M. Bastiaans, A.A. Konnov, L.P.H. de Goey, Experimental and modeling study of the effect of elevated pressure on lean high-hydrogen syngas flames, Proc. Combust. Inst. 35 (2015) 655–662.
[53] T. Kitagawa, T. Nakahara, K. Maruyama, K. Kado, A. Hayakawa, S. Kobayashi, Turbulent burning velocity of hydrogen–air premixed propagating flames at elevated pressures, Int. J. Hydrog. Energy 33 (2008) 5842–5849.
[54] X. Han, Z. Wang, Y. He, S. Wang, Y. Zhu, A.A. Konnov, Over-rich combustion of $CH_4$, $C_2H_6$, and $C_3H_8$ +air premixed flames investigated by the heat flux method and kinetic modeling, Combust. Flame 210 (2019) 339–349.

[55] O. Mathieu, E.L. Petersen, Experimental and modeling study on the high-temperature oxidation of ammonia and related NO*x* chemistry, Combust. Flame 162 (2015) 554–570.
[56] O. Mathieu, M.M. Kopp, E.L. Petersen, Shock-tube study of the ignition of multi-component syngas mixtures with and without ammonia impurities, Proc. Combust. Inst. 34 (2013) 3211–3218.
[57] J. Vandooren, J. Bian, P.J. Van Tiggelen, Comparison of experimental and calculated structures of an ammonia-nitric oxide flame. Importance of the $NH_2 + NO$ reaction, Combust. Flame 98 (1994) 402–410.
[58] Z. Tian, Y. Li, L. Zhang, P. Glarborg, F. Qi, An experimental and kinetic modeling study of premixed $NH_3/CH_4/O_2/Ar$ flames at low pressure, Combust. Flame 156 (2009) 1413–1426.
[59] J.W. Bozzelli, A.M. Dean, Energized complex quantum Rice-Ramsperger-Kassel analysis on reactions of amidogen with hydroperoxo, oxygen and oxygen atoms, J. Phys. Chem. 93 (1989) 1058–1065.
[60] R. Sumathi, D. Sengupta, M.T. Nguyen, Theoretical study of the $H_2 + NO$ and related reactions of $[H_2NO]$ isomers, J. Phys. Chem. A 102 (1998) 3175–3183.
[61] M. Goswami, R.J.M. Bastiaans, L.P.H. de Goey, A.A. Konnov, Experimental and modelling study of the effect of elevated pressure on ethane and propane flames, Fuel 166 (2016) 410–418.
[62] X. Han, Z. Wang, Y. He, Y. Liu, Y. Zhu, A.A. Konnov, The temperature dependence of the laminar burning velocity and superadiabatic flame temperature phenomenon for $NH_3$/air flames, Combust. Flame 217 (2020) 314–320.
[63] F. Liu, Ö.L. Gülder, Effects of pressure and preheat on super-adiabatic flame temperatures in rich premixed methane/air flames, Combust. Sci. Technol. 180 (2008) 437–452.
[64] M. Kumagami, Y. Ogami, Y. Tamaki, H. Kobayashi, Numerical analysis of extremely-rich $CH_4/O_2/H_2O$ premixed flames at high pressure and high temperature considering production of higher hydrocarbons, J. Therm. Sci. Technol. 5 (2010) 109–123.
[65] M. Goswami, S.C.R. Derks, K. Coumans, W.J. Slikker, M.H. de Andrade Oliveira, R.J.M. Bastiaans, C.C.M. Luijten, L.P.H. de Goey, A.A. Konnov, The effect of elevated pressures on the laminar burning velocity of methane+air mixtures, Combust. Flame 160 (2013) 1627–1635.
[66] K. Seshadri, X.S. Bai, H. Pitsch, Asymptotic structure of rich methane-air flames, Combust. Flame 127 (2001) 2265–2277.